

Formin-like 1 β phosphorylation at S1086 is necessary for secretory polarized traffic of exosomes at the immune synapse in Jurkat T lymphocytes

Reviewed Preprint

v3 • October 7, 2024


Revised by authors

Reviewed Preprint

v2 • August 22, 2024

Reviewed Preprint

v1 • April 23, 2024

Javier Ruiz-Navarro, Sara Fernández-Hermira, Irene Sanz-Fernández, Pablo Barbeito, Alfonso Navarro-Zapata, Antonio Pérez-Martínez, Francesc R Garcia-Gonzalo, Víctor Calvo, Manuel Izquierdo 

Instituto de Investigaciones Biomédicas Sols-Morreale (IIBM), CSIC-UAM, Madrid, Spain. • Departamento de Bioquímica, Facultad de Medicina, UAM, Madrid, Spain. • Translational Research in Pediatric Oncology, Hematopoietic Transplantation and Cell Therapy, IdiPAZ, La Paz University Hospital, Madrid, Spain. • Pediatric Onco-Hematology Clinical Research Unit, Spanish National Cancer Center (CNIO), Madrid, Spain. • Department of Pediatric Hemato-Oncology, La Paz University Hospital, Madrid, Spain. • Pediatric Department, Autonomous University of Madrid, Spain. • CIBER de Enfermedades Raras (CIBERER), Instituto de Salud Carlos III (ISCIII), Madrid, Spain. • Instituto de Investigación Sanitaria del Hospital Universitario La Paz (IdiPAZ), Madrid, Spain.

 https://en.wikipedia.org/wiki/Open_access

 Copyright information

Abstract

T-cell receptor stimulation (TCR) by antigen bound to the major histocompatibility complex (MHC) on an antigen-presenting cell (APC) induces protein kinase C (PKC) activation and the formation of the immune synapse (IS), followed by depletion of filamentous actin (F-actin) at the central region of the IS (cIS) and the polarization of multivesicular bodies (MVB) and the microtubule-organizing center (MTOC) to the IS. These events lead to polarized exosome secretion at the IS. These exosomes are involved in several crucial immune responses such as autocrine activation-induced cell death (AICD) of T lymphocytes and cytotoxicity. We analysed here how formin-like 1 β (FMNL1 β), an actin cytoskeleton-regulatory protein, regulates MTOC/MVB polarization and exosome secretion at an IS model in a phosphorylation-dependent manner. IS formation was associated with transient recruitment of FMNL1 β to the IS, which was independent of protein kinase C δ (PKC δ). Simultaneous RNA interference of all FMNL1 isoforms prevented MTOC/MVB polarization and exosome secretion, which were restored by FMNL1 β WT expression. However, expression of the non-phosphorylatable mutant FMNL1 β S1086A did not restore neither MTOC/MVB polarization nor exosome secretion to control levels, supporting the crucial role of S1086 phosphorylation in MTOC/MVB polarization and exosome secretion. In contrast, the phosphomimetic mutant, FMNL1 β S1086D, restored MTOC/MVB polarization and exosome secretion. Conversely, FMNL1 β S1086D mutant did not recover the deficient MTOC/MVB polarization occurring in PKC δ -interfered clones, indicating that S1086 FMNL1 β phosphorylation alone is not sufficient for MTOC/MVB polarization and exosome secretion. FMNL1 interference inhibited the depletion of F-actin at the cIS, which is necessary for MTOC/MVB polarization. FMNL1 β WT and FMNL1 β S1086D, but not FMNL1 β S1086A expression, restored F-actin depletion at the cIS. Thus, actin cytoskeleton reorganization at the IS underlies the effects of all these FMNL1 β

variants on polarized secretory traffic. FMNL1 was found in the IS made by primary T lymphocytes, both in TCR and chimeric antigen receptor (CAR)-evoked synapses. Taken together, these results point out a crucial role of S1086 phosphorylation in FMNL1 β activation, leading to cortical actin reorganization and subsequent control of MTOC/MVB polarization and exosome secretion.

eLife Assessment

This **important** study uses the Jurkat T cell model to study the role of Formin-like 1 β phosphorylation at S1086 on actin dynamics and exosome release at the immunological synapse. The evidence supporting these findings is **compelling** within the framework of the Jurkat model. As the Jurkat model is known to have a bias toward formin-mediated actin filament formation at the expense of Arp2/3-mediated branched F-actin foci observed in primary T cells, it will be beneficial in the future to confirm major findings in primary T cells.

<https://doi.org/10.7554/eLife.96942.3.sa2>

Introduction

T cell receptor (TCR) stimulation by antigen bound to major histocompatibility complex (MHC) molecules on the surface of an antigen-presenting cell (APC) induces the formation of the immune synapse (IS). The IS is a specialized cell-cell interface contact area that provides a signalling platform for integration of signals leading to intercellular information exchange, in order to ensure efficient TCR signal transduction, T cell activation and the proper execution of diverse T lymphocyte effector functions (1). Comprised among these functions, IS formation triggers the convergence of T lymphocyte secretory vesicles, including multivesicular bodies (MVB) (2) (3), towards the microtubule-organizing center (MTOC) and the polarization of MTOC together with secretory vesicles to the IS (4, 5). The canonical bullseye structure of a mature IS comprises three concentric areas referred to as supramolecular activation clusters (SMACs) that can be discerned based on the specific segregation of TCR, integrins and costimulatory molecules (6). The central supramolecular activation cluster (cSMAC) is enriched in ligand-bound TCR and associated signalling molecules, the peripheral SMAC (pSMAC) in adhesion molecules such as LFA-1, and the outer distal SMAC (dSMAC) in filamentous actin (F-actin) and CD45 (7) (8). IS assembly and subsequent secretory responses are coordinated by both actin and microtubule cytoskeletons, whose interplay regulates the polarized secretory response towards the IS (9) (7). IS formation is associated with an initial increase in cortical actin at the IS (10), followed by a decrease in cortical actin density at the central region of the immune synapse (cIS) including the cSMAC, that contains the secretory domain (11) (12). The partial depletion of F-actin at the cIS has been proposed, apart from allowing the focusing and docking of secretory vesicles for secretion (10), to initiate key subsequent events leading to MTOC polarization and delivery of secretory vesicles, such as lytic granules in cytotoxic T lymphocytes (CTL) (12) and cytokine-containing secretory vesicles in T-helper (Th) lymphocytes (13), to the secretory domain of the IS. The CTL degranulation of diverse secretory lytic granules with MVB structure results in the secretion to the synaptic cleft of Fas ligand (FasL)-containing exosomes (14) (15) (16) (17) (2) (18). These exosomes, along with perforin and granzymes, which are secreted in both soluble and nanoparticulate form in so-called supramolecular attack particles (SMAPs) (19) (20), lead to the induction of target cell apoptosis. In addition, FasL-containing exosomes have

been involved in autocrine FasL/Fas dependent, activation-induced cell death (AICD) produced upon TCR triggering (16 [↗](#)) (21 [↗](#)) (17 [↗](#)) (22 [↗](#)), an important immunoregulatory event involved in the downregulation of T cell immune responses (23 [↗](#)) (24 [↗](#)).

We have previously described that cortical actin reorganization at the IS plays an important role in MVB polarized traffic leading to exosome secretion in Th lymphocytes (25 [↗](#)) (26 [↗](#)) (3 [↗](#)). With respect to the molecular cues controlling this process, we have shown that TCR-stimulated protein kinase C δ (PKC δ) regulates cortical actin reorganization at the IS, thereby controlling MTOC/MVB polarization and ultimately leading to exosome secretion at the IS and AICD in Th lymphocytes (25 [↗](#)). Moreover, PKC δ is necessary for the polarization of lytic granules and the induction of cytotoxicity by mouse CTL (27 [↗](#), 28 [↗](#)), which supports a general role of PKC δ in secretory traffic leading to apoptosis in T lymphocytes. Besides PKC δ , several actin cytoskeleton regulators, including the formin FMNL1 and Diaphanous-1 (Dia1), also regulate MTOC polarization (29 [↗](#)) (30 [↗](#)) (31 [↗](#)). In this context, we have shown both PKC δ -dependent phosphorylation of FMNL1 at the IS and PKC δ -dependent F-actin clearing at the cIS, which participate in MTOC/MVB polarization leading to exosome secretion in CD4⁺ Jurkat T lymphocytes forming IS (25 [↗](#)) (26 [↗](#)) (3 [↗](#)). However, a formal connection between FMNL1 phosphorylation, F-actin regulation and MVB polarization/exosome secretion at the IS has not been established yet.

Regarding potential formin regulatory pathways, we have shown that FMNL1, but not Dia1, is strongly phosphorylated in T lymphocytes by PKC δ activators such as phorbol myristate acetate (PMA), but also upon TCR stimulation via an anti-TCR agonist as well as IS formation (26 [↗](#)). FMNL1 phosphorylation was inhibited in PKC δ -interfered T lymphocytes (26 [↗](#)), which is associated with a deficient MTOC polarization towards the IS (25 [↗](#)), supporting a PKC δ role in both FMNL1 phosphorylation and MTOC polarization (25 [↗](#)) (26 [↗](#)). Interestingly FMNL2, a related formin which exhibits a high homology with FMNL1, is phosphorylated by PKC α and, to a lower extent, by PKC δ , at S1072 (32 [↗](#)). This phosphorylation reverses FMNL2 autoinhibition mediated by interaction of N-terminal Diaphanous inhibitory domain (DID) with the C-terminal Diaphanous autoinhibitory domain (DAD), resulting in increased F-actin assembly, β 1-integrin endocytosis, invasive motility (32 [↗](#)) and filopodia elongation (33 [↗](#)). In this regard, recent evidence suggests that the mutation of a particular residue in FMNL2 impacting the DID-DAD interaction may result in functional implications for the characteristic actin-regulating activity of FMNL2, specifically in the context of podosome formation in macrophages (34 [↗](#)). Out of the three FMNL1 isoforms (α , β and γ) present in T lymphocytes and Jurkat cells (35 [↗](#)), S1086 in FMNL1 β is surrounded by a sequence displaying high homology to the one surrounding S1072 in FMNL2 (32 [↗](#)) (26 [↗](#)) (**Fig. 1** [↗](#)). Moreover, we have shown that FMNL1 β is the only FMNL1 isoform phosphorylated upon IS formation and capable of recovering MTOC polarization when it was reexpressed in cells simultaneously interfered for the three FMNL1 isoforms (26 [↗](#)). Thus, we hypothesize that IS-induced, PKC δ -dependent phosphorylation at S1086, a residue located within FMNL1 β DAD, may release the autoinhibition mediated by DID/DAD-interaction, thereby leading to the activation of FMNL1 β . Consequently, this activation would mediate the F-actin reorganization at the IS and the MTOC/MVB polarization, thereby enabling the subsequent exosome secretion. Here, we report that FMNL1 β phosphorylation at S1086 regulates F-actin reorganization leading to MTOC/MVB polarization and exosome secretion.

Results

FMNL1 interference and YFP-FMNL1 β variants expression

According to our previous data (26 [↗](#)), FMNL1 β plays a crucial role in MTOC polarization towards the IS. Moreover, we have also shown that FMNL1 β is strongly phosphorylated in T lymphocytes by PKC δ activators such as PMA, as well as by TCR stimulation and upon IS formation, which could potentially be related to FMNL1 β activation (26 [↗](#)). As previously stated, FMNL2 becomes active

upon PKC α phosphorylation at S1072, enhancing F-actin assembly (32) (33). In FMNL1 β , S1086 in arginine-rich DAD (labelled in Fig. 1) is surrounded by a sequence displaying high similarity to that around S1072 in FMNL2 (36) (32) (26) (Fig. 1A). Thus, we hypothesized that phosphorylation of FMNL1 β at S1086 may release DID-DAD auto-inhibition, thereby activating FMNL1 β and regulating MTOC polarization. To address this point, we introduced S1086A and S1086D mutations in the shFMNL1-HA-YFP-FMNL1 β construct (35) (26), which act as non-phosphorylatable and phosphomimetic residues, respectively (Fig. 1B). These resulting bicistronic vectors produce both FMNL1 interference and the corresponding YFP-FMNL1 β variant expression (35), acting as useful tools to analyse the role of FMNL1 β in IS formation during transient expression experiments (26). To confirm the previously described efficacy of these vectors (33) (26), we first analysed endogenous FMNL1 interference and YFP-FMNL1 β variants expression in C3 Jurkat clone transfected with the different vectors at the single cell level by immunofluorescence, using an anti-FMNL1 antibody that recognizes all its isoforms. This analysis was performed in transfected Jurkat cells forming synapses, to rule out any potential effect of IS formation and subsequent T lymphocyte activation on both endogenous FMNL1 interference and YFP-FMNL1 β variants expression. As seen in Fig. 2A, C3 cells transfected with the FMNL1 interfering plasmid shFMNL1-YFP (YFP⁺ cells) (second row), showed very low anti-FMNL1 signal when compared with non-transfected cells in the same preparation or control YFP⁻ cells (first row). In contrast, cells transfected with YFP-FMNL1 β WT, YFP-FMNL1 β S1086A or YFP-FMNL1 β S1086D (rows three to five, respectively), showed higher anti-FMNL1 fluorescence signals when compared to nontransfected cells in the same microscopy field (Fig. 2A). The Suppl. Fig. S1B shows, by single cell image analysis, that the mean fluorescence intensity (MFI) of the anti-FMNL1 in shFMNL1-YFP-expressing cells is extremely low when compared to the control YFP⁻ group, whereas it is much higher in YFP-FMNL1 β WT, YFP-FMNL1 β S1086A or YFP-FMNL1 β S1086D-expressing cells. As shown in Suppl. Fig. S1A, anti-FMNL1 MFI correlated with YFP-FMNL1 β MFI in YFP-FMNL1 β WT, YFP-FMNL1 β S1086A or YFP-FMNL1 β S1086D-expressing cells. To further verify this data, lysates from bulk populations of transfected cells were analysed by western blot (WB) using the same anti-FMNL1 antibody. The apparent molecular weights (MW) of the bands observed in the WB analysis were compatible with the predicted MW of endogenous FMNL1 (150 kDa) and the chimeric YFP-FMNL1 β variants (150 + 30 kDa) (Fig. 2B). The endogenous FMNL1 (150 kDa band) levels in lysates from cells transfected with YFP-FMNL1 β WT, YFP-FMNL1 β S1086A or YFP-FMNL1 β S1086D were lower than in control untransfected cells (Fig. 2B). The reduction of endogenous FMNL1 expression, as assessed by WB (between 40–80% reduction relative to control YFP⁻ cells), was apparently lower than that observed by single cell imaging analysis (compare panels A and B in Fig. 2 with Suppl. Fig. S1B). This is not surprising, since the transfection efficiency was relatively low (20–50%) and thus cell populations analysed by WB contained transfected as well as untransfected cells.

YFP-FMNL1 β WT is phosphorylated upon PKC activation but neither YFP-FMNL1 β S1086A nor YFP-S1086D are.

Once the different YFP-FMNL1 β variants were expressed, we analysed the ability of a PKC δ activator to induce their phosphorylation. To this end, we stimulated C3 clone transfected with the different constructs with the PKC δ activator PMA, which has been shown to induce strong FMNL1 phosphorylation (26). Subsequently, we immunoprecipitated FMNL1 with an anti-FMNL1 that recognises all FMNL1 isoforms (26) and analysed these immunoprecipitates (IPs) by WB with anti-phospho-Ser PKC substrate (32) (Fig. 3). In all the IPs from PMA-stimulated cells, anti-phospho-Ser PKC substrate detected a band corresponding to endogenous FMNL1 (150 kDa), which was 8- to 30-fold more intense than in IPs from unstimulated cells (Fig. 3, lower graph). In IPs from PMA-stimulated cells expressing YFP-FMNL1 β WT, anti-phospho-Ser PKC substrate detected an additional band of the predicted MW (150 + 30 kDa), which was also recognized by anti-FMNL1 (Fig. 3). However, in IPs from PMA-stimulated cells expressing YFP-FMNL1 β S1086A or S1086D no apparent phosphorylation of these FMNL1 β chimeras could be detected (Fig. 3). Thus,

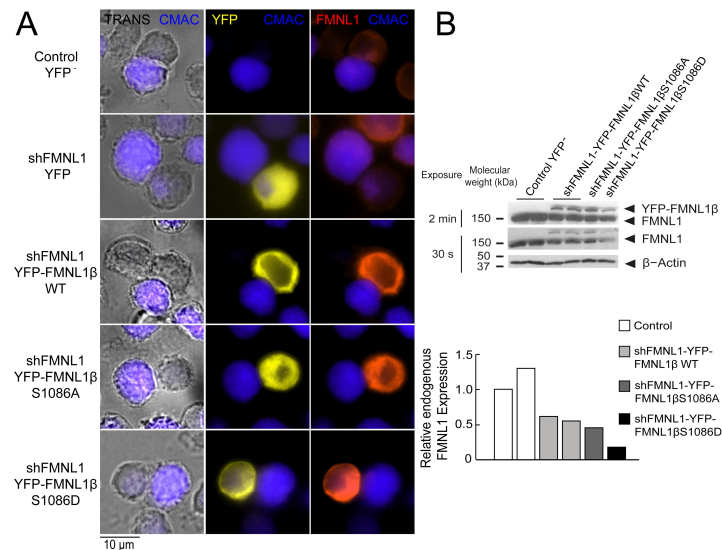


Fig. 2

Expression of YFP-FMNL1β S1086 variants in FMNL1-silenced cells.

Panel A), C3 control clone was untransfected (Control YFP⁻) (first row) or transfected with FMNL1-interfering (shFMNL1-HA-YFP) (second row), or FMNL1-interfering expressing interference-resistant YFP-FMNL1βWT (shFMNL1-HA-YFP-FMNL1βWT) (third row), YFP-FMNL1βS1086A (fourth row) or YFP-FMNL1βS1086D (fifth row) constructs. Subsequently, cells were challenged with CMAC-labelled SEE-pulsed Raji cells (blue) for 1 h, fixed, stained with anti-FMNL1, and imaged by epifluorescence microscopy. Representative MIP images of merged transmittance (TRANS), CMAC (blue), YFP (yellow), and anti-FMNL1 (red) channels are indicated for the different cell groups. Panel B), cell lysates corresponding to the indicated cell groups were analysed by WB developed with anti-FMNL1 antibody (two different expositions). The lower bar graph depicts the WB quantification showing the endogenous FMNL1 expression in the different cell groups relative to control untransfected (YFP⁻) cells. Results are representative of data from several independent experiments (n=3) with similar results.

substitution of S1086 by a non-phosphorylatable or a phosphomimetic residue fully abolished PKC δ activator-induced phosphorylation of FMNL1 β , as detected by anti-phospho-Ser PKC substrate, confirming our hypothesis that S1086 is indeed the residue that is phosphorylated in FMNL1 β upon PKC activation.

S1086 phosphorylation of FMNL1 β is crucial for MTOC/MVB polarization towards the IS

Next, we wanted to assess whether S1086 phosphorylation was related to FMNL1 β regulation of MTOC/MVB polarization towards the IS. To this end, untransfected (control YFP⁻) C3 cells, or transfected with the plasmids interfering all FMNL1 isoforms and expressing YFP (shFMNL1-YFP), YFP-FMNL1 β WT, YFP-FMNL1 β S1086A, or YFP-FMNL1 β S1086D (35) were challenged with SEE-pulsed Raji cells (blue). Next, we quantified MTOC/MVB polarization index (PI) in fixed synapses formed by the mentioned cell groups by epifluorescence microscopy and deconvolution, as previously described (37) (25) (26) (Suppl. Fig. S2A, Fig. 4). In the first series of experiments, average MTOC PI of untransfected (Control YFP⁻) C3 cells forming synapses with unpulsed Raji cells was significantly lower than with SEE-pulsed Raji cells, and similar to MTOC PI of FMNL1-interfered cells (shFMNL1-YFP) forming synapses with SEE-pulsed Raji cells (Suppl. Fig. S2B). This confirms that antigenic stimulation at the IS indeed triggers MTOC polarization and validates our synapse model measurements. In addition, confirming our previous data (26), MTOC/MVB polarization was disrupted upon FMNL1 interference to the levels obtained with unpulsed Raji cells (Fig. 4A, compare the first two rows, Fig. 4B, Suppl. Fig. S2B), and was restored by YFP-FMNL1 β WT expression (Fig. 4A, third row and 4B). Interestingly, non-phosphorylatable YFP-FMNL1 β S1086A expression was unable to restore MVB/MTOC polarization to control levels (Fig. 4A, fourth row and 4B), whereas phosphomimetic YFP-FMNL1 β pS1086D expression restored MVB/MTOC polarization to the levels achieved by YFP-FMNL1 β WT expression (Fig. 4A, fifth row and 4B). Comparable results were obtained by confocal microscopy (Suppl. Fig. S3). From confocal images, *en face* views of the IS interface were generated (Suppl. Fig. S4, S5 and Suppl. Videos 1 and 2). These images show the polarized MTOC or the polarized accumulation of MVB (measured as high MTOC and MVB PI values, in white types), respectively, in the cIS region of untransfected (control YFP⁻) C3 cells or cells expressing YFP-FMNL1WT or YFP-FMNL1S1086D, but not in cells transfected with shFMNL1-YFP or expressing YFP-FMNL1 β S1086A (low MTOC and MVB PI values). Thus, phosphorylation of S1086 in FMNL1 β appears to be essential for secretory polarized traffic towards the IS in T lymphocytes. Moreover, throughout the experiment, we observed that MTOC and MVB were polarizing together towards the IS. This fact, together with the previous work regarding segregation between MTOC movement and secretory granules traffic (13) (28, 38, 39), prompted us to simultaneously analyse both MTOC and MVB positioning with respect to the IS at the single cell level. Remarkably, we observed a robust linear correlation between MVB and MTOC PIs both in untransfected (control YFP⁻) C3 cells and cells transfected with shFMNL1-YFP (Pearson's linear correlation coefficients 0.96 and 0.95, respectively, Suppl. Fig. S6). Furthermore, it is noteworthy that MVB and MTOC centers of mass (MVB^C and MTOC^C, respectively) are very closely located in all the studied cell groups, regardless of polarization state (Fig. 4, Suppl. Fig. S3). Although the MTOC and MVB did not efficiently polarize in cells transfected with shFMNL1-YFP, their MVB^C were still located next to MTOC^C (Fig. 4A, second row), and equivalent results were obtained in all the analysed cell groups (Fig. 4). Thus, phosphorylation of S1086 in FMNL1 β appears to be essential for both MTOC and MVB polarization towards the IS in T lymphocytes.

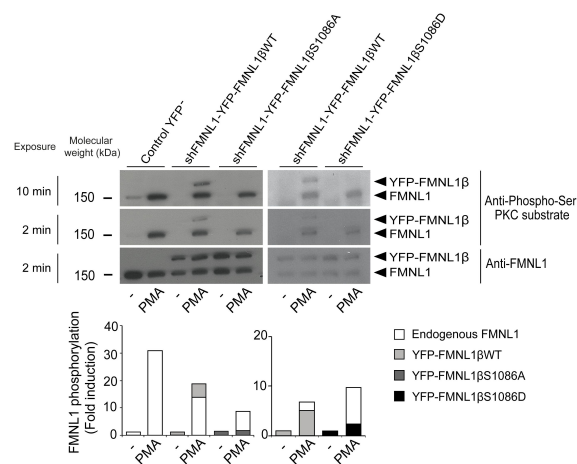


Fig. 3.

S1086 in FMNL1β is phosphorylated upon PKC activation.

C3 control clone was untransfected (Control YFP⁻) or transfected with either FMNL1-interfering expressing interference-resistant YFP-FMNL1βWT (shFMNL1-HA-YFP-FMNL1βWT), YFP-FMNL1βS1086A or YFP-FMNL1βS1086D constructs. Subsequently, cells were stimulated or not (-) with PKCδ activator PMA for 30 min. The different cell groups were lysed and immunoprecipitated with anti-FMNL1. These IPs were analysed by WB, first with anti-Phospho-Ser PKC substrate antibody (two different expositions) and then reprobed with anti-FMNL1 to normalize Phospho-Ser PKC substrate signal for FMNL1 protein levels. The lower graph represents the normalized fold induction of phosphorylation of the different FMNL1 variants. Results are representative of data from several independent experiments (n=3) with similar results.

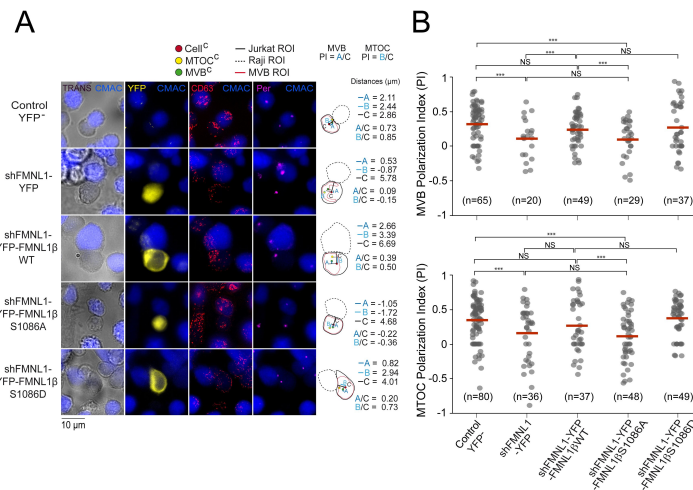


Fig. 4.

FMNL1 β phosphorylation at S1086 is involved in MTOC/MVB polarization towards the immune synapse.

C3 control clone was untransfected (Control YFP⁺) (first row) or transfected with FMNL1-interfering (shFMNL1-HA-YFP) (second row), or FMNL1-interfering expressing interference-resistant YFP-FMNL1 β WT (shFMNL1-HA-YFP-FMNL1 β WT) (third row), YFP-FMNL1 β S1086A (fourth row) or YFP-FMNL1 β S1086D (fifth row) constructs. Subsequently, cells were challenged with CMAC-labelled, SEE-pulsed Raji cells (blue) for 1 h, fixed, stained with anti-pericentrin (magenta) to label the MTOC and anti-CD63 (red) to label MVB, and imaged by epifluorescence microscopy. Panel A), representative MIP images with the indicated merged channels for each of the specified cell groups, along with a schematic diagram on the right representing the measured parameters used to calculate the MTOC and MVB PI. This includes the distance in microns between the MTOC^C (or MVB^C) projection on the vector defined by the Cell^C–synapse axis and the Cell^C (“B” or “A” distance, respectively), and the distance between the Cell^C and the synapse (“C” distance). Panel B), dot plots of MVB and MTOC PI from each of the indicated cell groups, corresponding to the indicated number of synapses from a experiment similar to that described in panel A) are depicted. NS, not significant. ***, $p \leq 0.05$. Results and ANOVA analyses are representative of data from several independent experiments ($n=3$) with similar results.

YFP-FMNL1 β S1086D phosphomimetic mutant expression does not rescue MTOC polarization in PKC δ -interfered T lymphocytes.

The former results supported the contribution of FMNL1 β and its phosphorylation at S1086 to MVB/MTOC polarization, but did not address the sufficiency in this process of PKC δ -controlled, S1086 FMNL1 β phosphorylation. In this context, we have previously shown that FMNL1 β lies downstream of PKC δ in the same pathway controlling MTOC/MVB polarization (26) (3). Thus, in order to analyse this important issue we transfected the PKC δ -interfered P5 and P6 clones with the different plasmids and compared the MTOC PI among the different cell groups, as previously done in C3 clone. We have previously shown that neither PKC δ nor FMNL1 interference affects IS conjugate formation, since P5 and P6 clones and FMNL1-interfered C3 clone formed IS with SEE-pulsed Raji cells (25) (26). In addition, IS formed by P5 clone with SEE-pulsed Raji cells (fifth group in **Suppl. Fig. S2B**) had a MTOC PI comparable to those of IS formed by C3 clone with unpulsed Raji cells or P5 clone with unpulsed Raji cells (first and fourth group, respectively, in **Suppl. Fig. S2B**), supporting that both FMNL1 or PKC δ interference fully inhibited MTOC polarization.

In contrast to what was found in the control C3 clone (**Fig. 4** and **Suppl. Fig. S3**) or C9 clone (not shown), YFP-FMNL1 β WT expression in PKC δ and FMNL1-interfered P5 clone (**Fig. 5**) or P6 clone (not shown) did not restore MTOC PI to the values observed in control YFP⁻ C3 cells, which is compatible with the idea that FMNL1 β lies downstream of PKC δ and its phosphorylation is indispensable for MTOC polarization. Consistently, expression in P5 clone of YFP-FMNL1 β S1086A, a variant non-phosphorylatable by PKC, was also unable to enhance MTOC PI to the values observed in control YFP⁻ C3 cells (**Fig. 5B**). Moreover, phosphomimetic YFP-FMNL1 β S1086D expression, which restored MVB/MTOC PI to the values achieved by YFP-FMNL1 β WT expression in the C3 clone (**Fig. 4** and **Suppl. Fig. S3**), did not restore MTOC PI in PKC δ and FMNL1-interfered P5 cells to the levels observed in control YFP⁻ C3 cells (**Fig. 5B**). Similarly, FMNL1 β S1086D expression was unable to revert the deficient MTOC polarization occurring in P6 (not shown), a different PKC δ -interfered clone previously described (25). We have shown that the deficient MTOC/MVB polarization in the PKC δ -interfered P5 and P6 clones is due exclusively to the reduction in PKC δ expression, since transient re-expression of PKC δ in all these clones recovered MTOC/MVB polarization to control levels (25). Since both the FMNL1 interference and FMNL1 variant re-expression for IS experiments were performed in transient assays (2–4 days after transfection), there was no chance for any clonal variation in these short-time experiments. Taken together, these results show that although FMNL1 β phosphorylation at S1086 is necessary, it does not seem to be sufficient for MTOC polarization, at least in cells lacking PKC δ .

FMNL1 β translocation to the immune synapse is independent of S1086 phosphorylation and PKC δ .

Previous results have shown that FMNL1, apart from being mainly located at the cytosol and centrosomal areas, was also found located at the IS in a small percentage of synaptic conjugates, in end-point IS experiments (29) (26). If confirmed, the possibility of an IS-induced FMNL1 translocation to the IS may provide the molecular basis underlying a potential regulatory effect of FMNL1 on cortical actin cytoskeleton reorganization at the IS as well as on MTOC/MVB and secretion granule polarization, occurring both in CTL and Th cells, as suggested by several authors (9, 12) (13) (40) (3). However, although it could be inferred (29) (41) that the active translocation of any FMNL1 isoform from cytosol towards the IS is induced upon IS formation, it has not been formally demonstrated yet (29) (41). This is probably due to the fact that most early studies have used an end-point approach that does not allow to analyse the incipient IS (29) (42) (43) (44). Since FMNL1 β is responsible for MTOC/MVB polarization to the IS (44), we analysed FMNL1 β subcellular location in developing synapses by time-lapse,

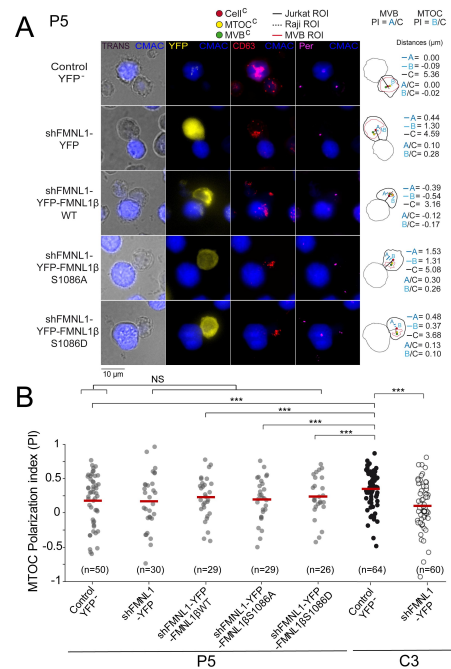


Fig. 5.

YFP-FMNL1βS1086D expression does not rescue deficient MTOC polarization in PKCδ-interfered cells.

PKCδ-interfered P5 clone was untransfected (Control YFP⁻) (first row) or transfected with FMNL1-interfering (shFMNL1-HA-YFP) (second row), FMNL1-interfering expressing interference-resistant YFP-FMNL1βWT (shFMNL1-HA-YFP-FMNL1βWT) (third row), YFP-FMNL1βS1086A (fourth row) or YFP-FMNL1βS1086D (fifth row) constructs. In parallel, C3 control clone was untransfected (Control YFP⁻) or transfected with FMNL1-interfering (shFMNL1-HA-YFP) construct. Subsequently, cells were challenged with CMAC-labelled, SEE-pulsed Raji cells (blue) for 1 h, fixed, stained with anti-pericentrin (magenta) to label the MTOC and anti-CD63 (red) to label MVB, and imaged by epifluorescence microscopy. Panel A), representative MIP images with the indicated merged channels for each of the specified cell groups along with their corresponding diagrams as in **Fig. 4**, representing the measured parameters used for calculating the MTOC and MVB PI are shown. This includes the distance in microns between the MTOC^C (or MVB^C) projection on the vector defined by the Cell^C-synapse axis and the Cell^C ("B" or "A" distance, respectively), and the distance between the Cell^C and the synapse ("C" distance). Panel B), dot plots of MTOC PI of each cell group. Untransfected (Control YFP⁻) and FMNL1-interfering (shFMNL1-HA-YFP) C3 clone synapses corresponding to the data shown in **Suppl. Fig. S3B** were included in the far-right columns, as a reference. NS, not significant; ***, $p \leq 0.05$. Results and ANOVA analyses are representative of data from several independent experiments (n=3) with similar results.

epifluorescence microscopy (43) (44). For this analysis, FMNL1-interfered, YFP-FMNL1 β WT-expressing C3 clone was challenged with SEE-pulsed Raji cells. As evidenced in the example shown in Suppl. Video 3 (upper panel) and Fig. 6A (upper row), a transient relocation of initially cytosolic YFP-FMNL1 β WT to the IS (white arrow) was observed in these cells. The average (\pm SD) duration of YFP-FMNL1 β WT accumulation at the IS in C3 clone was around 6 min (6 min 18 s \pm 1 min 34 s, n=6 synapses).

Considering the major role of PKC α in FMNL2 relocation from the plasma membrane to the endosomal membrane (32), the high similarity between FMNL2 and FMNL1 β C-terminal regions (Fig. 1) and the reported PKC δ -mediated FMNL1 β phosphorylation (26), we next aimed to analyse the role of PKC δ in YFP-FMNL1 β WT translocation to the IS. To this end we analysed YFP-FMNL1 β WT translocation upon IS formation in the PKC δ -interfered P5 clone (25) (Suppl. Video 3 and Fig. 6A). The results in P5 clone showed a clear translocation of YFP-FMNL1WT to the IS (white arrow), with an accumulation of around 8 minutes at the IS (8 min 55 s \pm 3 min 2 s, n=6 synapses, not significant differences with the C3 clone), so YFP-FMNL1 β WT translocation to the IS in P5 and C3 clones showed comparable kinetics.

Moreover, to directly analyse the specific involvement of S1086 phosphorylation in this process, we challenged FMNL1-interfered, YFP-FMNL1 β S1086A and YFP-FMNL1 β S1086D-expressing C3 cells with SEE-pulsed Raji cells. As shown in Suppl. Video 4 and Suppl. Fig. S8, both YFP-FMNL1 β S1086A and YFP-FMNL1 β S1086D transiently relocated to the IS. The average time of YFP-FMNL1 β S1086A accumulation at the IS was around 7 min (7 min 30 s \pm 1 min 58 s, n=6 synapses), whereas YFP-FMNL1 β S1086D showed an average accumulation time of around 6 min (6 min 52 s \pm 2 min 9 s, n=7 synapses; not significant differences between YFP-FMNL1 β S1086A and YFP-FMNL1 β S1086D, nor between any of the mutants and YFP-FMNL1 β WT). Therefore, these results confirm that the translocation and accumulation of FMNL1 β in the IS region of Jurkat cells is a process that occurs independently of both PKC δ and S1086 FMNL1 β phosphorylation.

A more detailed study of subsynaptic location of endogenous FMNL1 in C3 control clone using fixed synapses demonstrated that FMNL1 accumulated at the cIS but also at the edges of the synapse, around the dSMAC, both in C3 control clone (Fig. 6B, first and second rows, respectively) and in P5 PKC δ -interfered clone (Fig. 6B, third and fourth rows). At these subsynaptic locations, FMNL1 colocalized with F-actin (white pixels), which is compatible with the idea that FMNL1 regulates F-actin at the IS. To extend these results obtained in Jurkat cells we have performed experiments using primary T cells developing synapses mediated by TCR recognizing SEE plus SEB superantigens and a dual chimeric antigen receptor (CAR) recognizing CD19/CD22 on Raji cells (Suppl. Fig. S7A and B, respectively). As shown in this figure, endogenous FMNL1 colocalizing with F-actin at the IS was also found in both types of synapses developed by primary T lymphocytes.

Subsequently, we studied the subsynaptic locations of YFP-FMNL1 β WT, YFP-FMNL1 β S1086A, and YFP-FMNL1 β S1086D in C3 control clone, to identify whether S1086 phosphorylation affected these locations. The results from fixed synapses, obtained through both epifluorescence (Suppl. Fig. S8 and S9) and confocal microscopy (Suppl. Fig. S10), revealed the presence of accumulations of the three YFP-FMNL1 β variants in the IS. Additionally, in Suppl. Fig. S10, it can be observed that the three YFP-FMNL1 β variants colocalized with F-actin at the IS.

Taken together, these observations show that, upon IS formation, FMNL1 β translocates to the IS, with both PKC δ and S1086 phosphorylation being dispensable for the translocation to the IS of both endogenous FMNL1 and YFP-FMNL1 β variants.

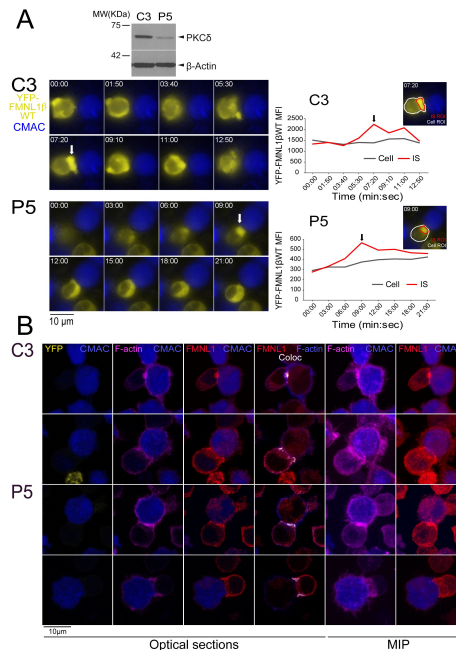


Fig. 6.

FMNL1 β recruitment to the immune synapse is PKC δ -independent.

C3 control and P5 PKC δ -interfered cells were transfected with FMNL1-interfering expressing interference-resistant YFP-FMNL1 β WT (shFMNL1-HA-YFP-FMNL1 β WT) plasmid. Subsequently, both transfected clones were simultaneously challenged with CMAC-labelled, SEE-pulsed Raji cells (blue) attached to slides and time-lapse acquisition of emerging synapses was performed as indicated in Materials and Methods. The videos (7 fps) ([Suppl. Video 3](#)) were captured and in panel A), left, representative frames from videos of each clone are shown. White arrows indicate accumulations of YFP-FMNL1 β WT at the IS. WB analysis of cell lysates from both clones (top inset) shows PKC δ silencing in P5 clone. In the right side, YFP-FMNL1 β WT MFI within the cell ROI (grey line) and the IS ROI (red line) are represented. The inserts in the graphs include the cell ROI (white) and the IS ROI (red) used for the time-lapse measurements on representative frames for both clones. Results are representative of the data from several videos (n=6 for each clone) with similar results. Panel B), control C3 (upper rows) and P5 PKC δ -interfered cells (lower rows) were simultaneously challenged with CMAC-labelled SEE-pulsed Raji cells (blue) attached to slides. After 1 h, synapses were fixed and immunofluorescence developed with anti-FMNL1 (red) to label endogenous FMNL1 and phalloidin (magenta) to label F-actin. Synapses were imaged with confocal fluorescence microscopy and colocalization pixels between FMNL1 (red) and F-actin (acquired in magenta, changed to blue in the fourth column) are represented in white. Representative optical sections of synapses formed by both clones are shown in the left columns. The colocalization coefficients were: First row, Pearson= 0.50, Manders= 0.877; Second row, Pearson = 0.431, Manders= 0.864; Third row: Pearson= 0.434, Manders= 0.838; Fourth row, Pearson= 0. 484, Manders= 0.794. MIP images of the same synapses are shown in the two far right columns. Results and ANOVA analyses are representative of data from several independent experiments (n=3) with similar results.

S1086 phosphorylation of FMNL1 β is necessary for cortical F-actin reorganization during MTOC/MVB polarization

The observations that YFP-FMNL1 β translocated to the IS, that cortical F-actin remodelling was considered to be sufficient for centrosome polarization in CTL (12), and that cortical F-actin remodelling was associated with MTOC and secretory granule polarization in CD4⁺ cells (13) (45), prompted us to study a potential role of FMNL1 β and its phosphorylation at S1086 in synaptic F-actin architecture. To address this point, fixed synapses formed by the C3 clone transfected with the previously described plasmids were stained with phalloidin AF647 to label F-actin and imaged by confocal fluorescence microscopy. The relative area of the F-actin-low region at the cIS (Fact-low cIS area / IS area) in the IS interface, which mirrors cortical F-actin reorganization at the IS, was measured as indicated in Materials and Methods and represented for all cell groups. As seen in a representative example in Fig. 7A, the dot plot in Fig. 7B and Suppl. Video 5, the F-actin-low region at the cIS was smaller in FMNL1-interfered cells than in untransfected control YFP⁻ cells (Fig. 7A, second and first columns, respectively), as it was also in PKC δ -interfered cells (25) (26). Of note, YFP-FMNL1 β WT expression restored F-actin depletion at the cIS to control levels (Fig. 7B). In contrast, YFP-FMNL1 β S1086A expression did not rescue F-actin depletion to control levels, whereas YFP-FMNL1 β S1086D did (Fig. 7B). Thus, FMNL1 β phosphorylation at S1086 appears to be necessary for F-actin reorganization at the IS, as it was for MTOC/MVB polarization (Fig. 4).

Three-dimensional FMNL1 β distribution at the synapse

We observed a positive effect of FMNL1 β phosphorylation at S1086 on cortical F-actin rearrangement at the IS (former paragraph and Fig. 7) and YFP-FMNL1 β translocated to the cIS, but also to the dSMAC (Suppl. Video 3 and 4, Fig. 6 and Suppl. Fig. S8, S9 and S10). To investigate this further, we analysed in more detail the subsynaptic distribution of the endogenous FMNL1, YFP-FMNL1 β WT, and the YFP-FMNL1 β S1086A and S1086D mutants with respect to the actin cytoskeleton. To this end, fixed synapses formed by the C3 clone transfected with the different plasmids were stained with phalloidin, anti-FMNL1 and anti-phospho-Ser PKC substrate antibody and imaged by confocal fluorescence microscopy (Suppl. Videos 6 and 7, Fig. 8 and Suppl. Fig. S11). Figs. 8A and 8B show representative examples of synaptic conjugates yx views (first row) and cropped synapse areas (white rectangles in first row) used to generate zx IS interfaces (second row), as shown in Suppl. Video 6 and 7. Subsequently, the colocalization pixels (white) along all the Z-stack at the IS interface (interface colocalization) were determined as indicated in Materials and Methods. This involved merging the indicated fluorescence channels (Fig. 8A, second row, F-actin in blue and anti-FMNL1 in red; Fig. 8B, second row, F-actin in blue and YFP fluorescence in green) on the IS interfaces of the synaptic areas generated as shown in Suppl. Video 6. MFI profile of each channel (F-actin in blue, anti-FMNL1 in red, YFP in green and colocalization in grey) along the indicated white arrows are shown below each IS interfaces. As shown in Fig. 8, and consistently with results from Fig. 7, both control YFP⁻ (first column) and YFP-FMNL1 β WT-expressing cells (third and fourth columns) exhibited a wide F-actin depletion area at the cIS and an F-actin accumulation at the dSMAC. Interestingly, in some synapses from control YFP⁻ (first column) and YFP-FMNL1 β WT-expressing cells (fourth column), F-actin and FMNL1 colocalized (white pixels) at certain small areas at the wide F-actin-low region at the cIS, although the MFI profiles show relatively less F-actin and FMNL1 at the cIS than at the dSMAC. In other synapses from both control YFP⁻ (not shown) and YFP-FMNL1 β WT-expressing cells (third column), F-actin and FMNL1 colocalization occurred at the F-actin rich-area corresponding to the dSMAC (Fig. 8A), which was consistent with the data from Fig. 6B. In contrast, and consistently with Fig. 7, FMNL1-interfered cells (Fig. 8, second column) displayed small F-actin low areas at the cIS. Moreover, synapses from YFP-FMNL1 β S1086A-expressing cells (fifth column) did not exhibit the F-actin depletion at the cIS, whereas synapses from the YFP-FMNL1 β S1086D-expressing cells (sixth column) exhibited wide F-

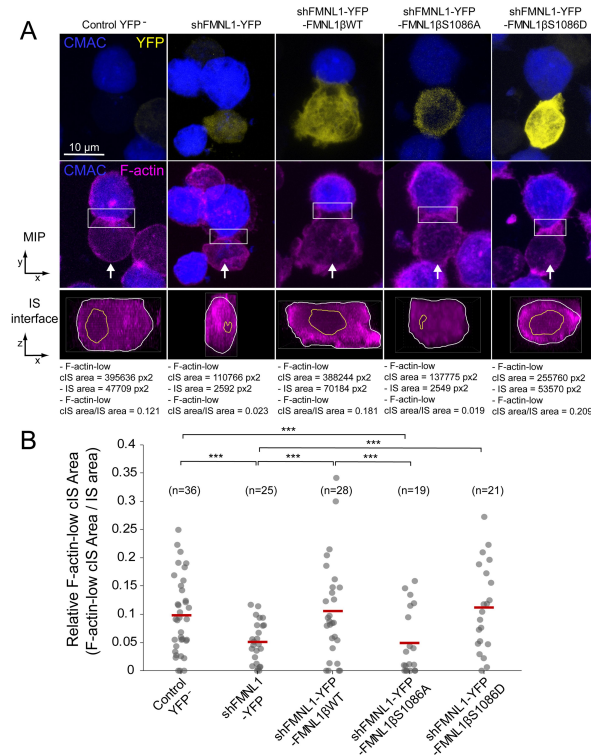


Fig. 7.

FMNL1β phosphorylation at S1086 regulates the F-actin architecture of the immune synapse.

C3 control clone was untransfected (Control YFP⁻) (first column) or transfected with FMNL1-interfering (shFMNL1-HA-YFP) (second column), FMNL1-interfering expressing interference-resistant YFP-FMNL1βWT (shFMNL1-HA-YFP-FMNL1βWT) (third column), YFP-FMNL1βS1086A (fourth column) or YFP-FMNL1βS1086D (fifth column) constructs. Subsequently, cells were challenged with CMAC-labelled, SEE-pulsed Raji cells (blue) for 1 h, fixed, stained with phalloidin AF647 (magenta) to label F-actin, and imaged by confocal microscopy. Panel A), the upper rows display the top, yx views corresponding to the MIP images of the specified, merged channels of a representative example from each of the indicated cell groups. White arrows indicate the direction to visualize the *en face* views of the IS (IS interface) enclosed by the ROIs (white rectangles), as shown in **Suppl. Video 5**. In the lower panels, the enlarged ROIs (2x zoom) used to generate the IS interface, zx images of each cell group are shown. The areas of the F-actin-low region at the cIS (Fact-low cIS area) (yellow line) and the synapse (IS area) (white line) were defined and measured as indicated in Materials and Methods, and the relative area of the F-actin-low region at the cIS (Fact-low cIS area / IS area) was calculated and represented. Panel B), relative area (Fact-low cIS area / IS area) dot plot distributions and average area ratios (red horizontal lines) for the indicated number of IS conjugates developed by each cell group are shown. This figure is related to **Suppl. Video 5**. NS, not significant; ***, $p < 0.05$. Results are representative of data from several independent experiments ($n = 3$) with similar results.

actin depletion at the cIS, comparable to those observed in the control YFP⁻ and in the YFP-FMNL1 β WT-expressing cells (Fig. 8 [↗](#)). In cells expressing the YFP-FMNL1 β variants, colocalization of all the YFP-FMNL1 β variants with F-actin was mainly in the F-actin low area at the cIS or at the dSMAC. When colocalization in all Z optical sections was assessed using directly the YFP fluorescence construction instead of anti-FMNL1 signal (Fig. 8B [↗](#), second row, F-actin in blue and YFP fluorescence in green), comparable results were obtained. In addition, we analysed the subsynaptic location of FMNL1 with respect to Ser-phosphorylated PKC substrates by using an anti-FMNL1 and an anti-phospho-Ser PKC substrate. The last antibody was validated by WB, both on endogenous FMNL1 and FMNL1 β variants (Fig. 3 [↗](#)). Moreover, the phospho-PKC does not recognize YFP-FMNL1 β S1086A or S1086D variants (Fig. 3 [↗](#)). In addition, when FMNL1 is interfered, the phospho-PKC does not colocalize with FMNL1 and it strongly colocalizes at the synapse with expressed YFP-FMNL1 β WT (Fig. S11 [↗](#)) in the Jurkat cell. Taken together these results indeed demonstrate the specificity of phospho-PKC antibody and that this antibody certainly recognizes phosphorylated FMNL1 β in the Jurkat cell.

Both endogenous FMNL1 in control YFP⁻ cells (Suppl. Video 7 [↗](#) and Suppl. Fig. S11A [↗](#), first column) and YFP-FMNL1 β WT in YFP-FMNL1 β WT⁺ cells, (Suppl. Fig. S11A [↗](#), third column) strongly and specifically colocalized with anti-phospho-Ser PKC substrate at the cIS. This is evidenced by the accumulation of white, colocalization pixels at low FMNL1 density areas located at the cIS, which is also an F-actin-low area (Fig. 8 [↗](#), see MFI profiles for control YFP⁻ and YFP-FMNL1 β WT⁺ cells). When colocalization at the synapse interface was assessed using directly the YFP fluorescence construction instead of anti-FMNL1 signal (Suppl. Fig. S11B [↗](#) second row, anti-phospho-Ser PKC substrate in blue and YFP construction in green and Suppl. Video 7 [↗](#)) comparable results were obtained. In addition, as expected and as a negative control, no colocalization of FMNL1 and anti-phospho-Ser PKC substrate was observed in FMNL1-interfered cells (Suppl. Fig. S11 [↗](#) and Suppl. Video 7 [↗](#), second column). Moreover, FMNL1 and anti-phospho-Ser PKC also colocalized using super resolution STED microscopy, that greatly reduces xy resolution limits down to 30 nm (Suppl. Fig. S12 [↗](#)). Although all these data do not yet allow us to infer that FMNL1 β is phosphorylated at the IS due to the resolution limits of super resolution microscopy and the possibility that another PKC substrate may be associated to FMNL1 or very close to FMNL1, in a strictly S1086-dependent manner, the results are compatible with the idea that both endogenous FMNL1 and YFP-FMNL1 β WT are specifically phosphorylated at the cIS.

S1086 phosphorylation of FMNL1 β regulates exosome secretion

The aforementioned results support that FMNL1 β and its phosphorylation at S1086 are involved in MTOC/MVB polarized traffic to the IS, most probably via control of F-actin rearrangement at the IS. MVB transport and fusion to the plasma membrane are necessary for exosome secretion ([46](#) [↗](#)) ([22](#) [↗](#)) and PKC δ controls F-actin depletion at the cIS ([25](#) [↗](#)), thus, it is conceivable that FMNL1 β may control subsequent exosome secretion at the IS. To directly analyse FMNL1 β contribution to exosome secretion, we used an exosome secretion reporter assay. We transiently cotransfected C3 clone with the exosome reporter GFP-CD63 expression plasmid ([2](#) [↗](#)) ([47](#) [↗](#)) and the different shFMNL1-YFP constructs. Subsequently, IS were formed between the cotransfected C3 clone and SEE-pulsed Raji cells, exosomes were purified from cell culture supernatants ([2](#) [↗](#)), lysed, and exosome lysates were analysed by anti-CD63 WB. This secretion assay excludes the detection of exosomes released by Raji cells in the coculture, that otherwise may mask the exosomes released by Jurkat cells ([2](#) [↗](#)) ([22](#) [↗](#)). In parallel, we determined nanovesicle concentrations in coculture supernatants by using Nanoparticle Tracking Analyses (NTA) (Fig. 9A [↗](#)). Anti-CD63 WB analysis of exosome secretion is shown in Fig. 9B [↗](#). We normalized exosomal GFP-CD63 signal to the transfection efficiency of the exosome reporter (measured by GFP-CD63 signal from cell lysates) and the number of viable exosome-secreting cells (Fig. 9B [↗](#)). As shown in Fig. 9 [↗](#), interference with all FMNL1 isoforms not only reduced exosomal GFP-CD63 levels, but also reduced SEE-stimulated nanovesicle concentration increase. These results mirrored those obtained in cells in PKC δ -interfered cells ([25](#) [↗](#)). Moreover, interference with all FMNL1 isoforms and YFP-FMNL1 β WT expression recovered exosome secretion to the levels produced by control YFP⁻ cells.

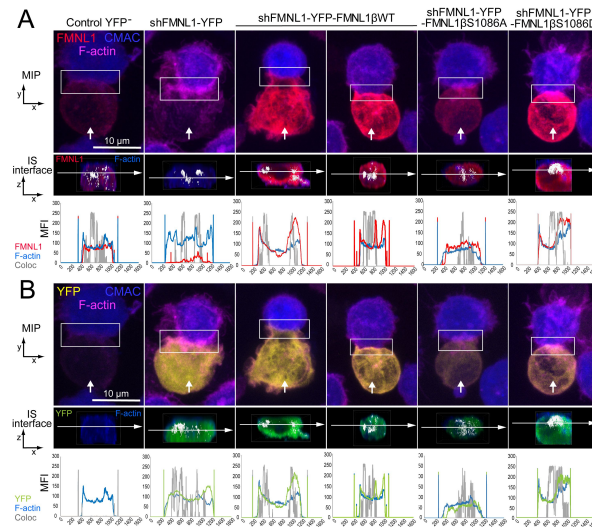


Fig. 8.

Three-dimensional distribution and colocalization of FMNL1 and F-actin at the immune synapse interface.

C3 control clone was untransfected (Control YFP⁺) (first column) or transfected with FMNL1-interfering (shFMNL1-HA-YFP) (second column), FMNL1-interfering expressing interference-resistant YFP-FMNL1 β WT (shFMNL1-HA-YFP-FMNL1 β WT) (third and fourth column), YFP-FMNL1 β S1086A (fifth column) or YFP-FMNL1 β S1086D (sixth column) constructs. Subsequently, cells were challenged with CMAC-labelled SEE-pulsed Raji cells (blue) for 1 h, fixed, and stained with phalloidin (magenta) and anti-FMNL1 (red). The corresponding shFMNL1 construction is in yellow, and synaptic conjugates were imaged by confocal fluorescence microscopy. Please realize that for the IS interface and since interface colocalization in NIS-AR only works with red, green and blue channels, F-actin (acquired in magenta) was changed to blue color, and YFP (acquired in yellow) was changed to green in the second row of each panel. Panel A), the upper row includes top, yx views corresponding to the MIP images of representative examples of each cell group. Vertical white arrows indicate the direction to visualize the *en face* views of the IS (IS interface) enclosed by the ROIs (white rectangles), as shown in [Suppl. Video 6](#). In the second row, the enlarged ROIs (2x zoom) used to generate the IS interface, zx images of each cell group are shown. Subsequently, interface colocalization pixels (white) were generated by merging the indicated channels in the second row of each panel (F-actin in blue merged to anti-FMNL1 in red), at the IS interfaces of the synaptic areas (generated as shown in [Suppl. Video 6](#)). The last frame of these videos corresponds to the *en face* view (interface) (second row in both panels). MFI profiles along the indicated line (horizontal white arrow) of each separate channel (F-actin in blue, anti-FMNL1 in red) and the colocalization pixels (grey) are shown below the IS interfaces. Panel B), same as panel A, but the top views show YFP-expressing constructs signal instead of the anti-FMNL1 signal. The IS interfaces and the MFI profiles show F-actin (magenta changed to blue) and YFP (yellow changed to green). This figure is related to [Suppl. Video 6](#). At least 6 synapses of each cell group were analysed. Results are representative of data from several independent experiments (n=3) with similar results.

However, YFP-FMNL1 β S1086A expression did not recover exosome secretion, whereas YFP-FMNL1 β S1086D expression rescued exosome secretion to the values observed in control YFP⁺ or YFP-FMNL1 β WT-expressing cells (**Fig. 9B**). These results demonstrate IS-induced exosome secretion, but do not reveal the presence of exosomes at the synaptic cleft. Therefore, we have performed STED super-resolution imaging of the immune synapses made by control and FMNL1-interfered cells. Nanosized (100–150 nm) CD63⁺ vesicles can be found in the synaptic cleft between the APC and control YFP⁺ cells with polarized MVB, whereas we could not detect these vesicles in the cleft from FMNL1-interfered cells that maintain unpolarized MVB (**Fig. 10**). Taken together, these results on exosome secretion endorse the outcomes regarding FMNL1 interference and FMNL1 β -mediated control of cortical F-actin reorganization at the IS and their role on MVB polarized secretory traffic.

Discussion

Our previously published results suggest that PKC δ -dependent phosphorylation of FMNL1 β may regulate its function in F-actin reorganization at the IS and hence affect MTOC polarization (25) (26). We have previously shown that phosphorylation occurs in FMNL1 but not in a homologous formin, Dia1 (26), that also regulate MTOC polarization and it is a major actin regulator in T lymphocytes (29), supporting a specific role of FMNL1 phosphorylation, but not Dia1 phosphorylation on MTOC polarization. Here, we have identified for the first time a positive regulatory role of FMNL1 β phosphorylation at S1086 in cortical F-actin regulation that governs MTOC/MVB polarization and exosome secretion at the IS in Th lymphocytes. Moreover, the fact that the phosphomimetic YFP-FMNL1 β S1086D expression in PKC δ and FMNL1-interfered cells, did not recover the MTOC PI observed in C3 control cells (**Fig. 5**) supports the idea that FMNL1 β phosphorylation at S1086 is necessary but not sufficient for MTOC polarization, at least in cells lacking PKC δ . Thus, these results support that another signal, apart from PKC δ activation, or another PKC δ -controlled pathway not involving FMNL1 β phosphorylation, evoked upon TCR triggering at the IS, is also implicated in MTOC/MVB polarization to the IS.

Our results on FMNL1 β phosphorylation are certainly related to what was found in formin homology domain protein 1 (FHOD1) regulation. FHOD1 is grouped into Dia-related formins (48). FHOD1 requires active Rac to be recruited to the plasma membrane, but its recruitment appears insufficient for FHOD1 activation, which is achieved only after being phosphorylated by Rho-dependent protein kinase (ROCK) at three serine and threonine sites included in a polybasic arginine-rich region inside the C-terminal DAD (49), leading to disruption of FHOD1 autoinhibitory state and F-actin stress fiber formation (49). This activation process is similar to what we have described in this article for FMNL1 β . Moreover, the PKC-dependent mode of FMNL2 activation during integrin activation (32) and filopodia formation (33) is comparable to what we have found in FMNL1 β during polarized traffic to the IS. Furthermore, FHOD3 formin is also autoinhibited by an intramolecular interaction between its C- and N-terminal domains. Phosphorylation of the three highly conserved residues (S1406, S1412, and T1416) within the polybasic, C-terminus of FHOD3 by ROCK1/2 is sufficient for its activation and is crucial in regulating myofibrillogenesis in cardiomyocytes (50). Thus, with the results provided here for FMNL1 β , it has been reported that at least four different formins are activated through phosphorylation by three different kinases at the C-terminal polybasic regions, which are included in a common DAD. This underscores the evolutionary importance of this regulatory mechanism in formin activation, ultimately leading to very diverse cellular responses. However, although we do not have conclusive evidence supporting that PKC directly phosphorylates FMNL1 β , the presence of a conserved S1086 within a RRSV/AR motif that contains a potential target for classical PKCs (32, 33, 51), along with the recognition of the phosphorylated residue by a validated anti-Phospho-Ser PKC substrate antibody (32), certainly support this possibility.

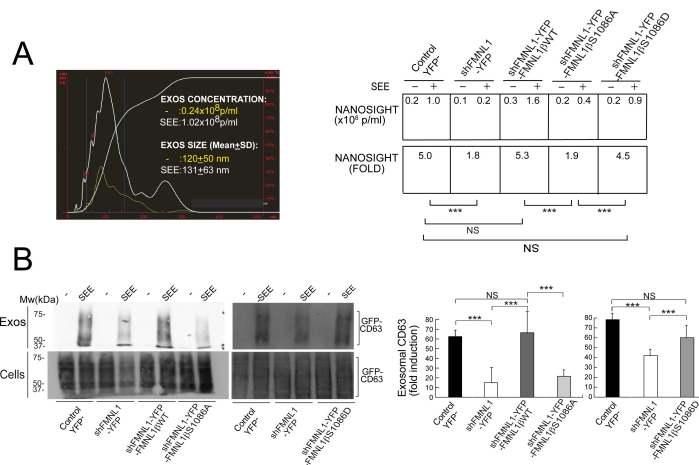


Fig. 9.

FMNL1β phosphorylation at S1086 regulates exosome secretion at the immune synapse.

C3 control clone was transfected with exosome reporter GFP-CD63 alone (Control YFP⁻) or co-transfected with the exosome reporter GFP-CD63 and 3-fold molar excess of either FMNL1-interfering (shFMNL1-HA-YFP), or FMNL1-interfering expressing interference-resistant YFP-FMNL1βWT (shFMNL1-HA-YFP-FMNL1βWT), YFP-FMNL1βS1086A or YFP-FMNL1βS1086D constructs. Subsequently, the different cell groups were challenged with unpulsed (-) or SEE-pulsed Raji cells for 4 h and exosomes were collected and purified from cell culture supernatants and analysed by NTA and WB, as indicated in Materials and Methods. Panel A), left, NTA analyses corresponding to nanovesicles isolated from cell culture supernatants of control YFP⁻ Jurkat cells stimulated with unpulsed Raji cells (-) or SEE-pulsed Raji cells (SEE). Right, concentration and SEE-stimulated nanoparticle concentration increase (fold) induction of secreted nanovesicles from several NTA analyses for the indicated cell groups. Panel B), left, WB analyses of exosomal GFP-CD63 reporter isolated from the indicated cell culture supernatants. Right, quantification of normalized, fold induction of exosomal GFP-CD63 secretion from three experiments similar to the one described in the left panel. NS, not significant; ***, $p \leq 0.05$. Results and ANOVA analyses are representative of data from several independent experiments ($n=3$) with similar results.

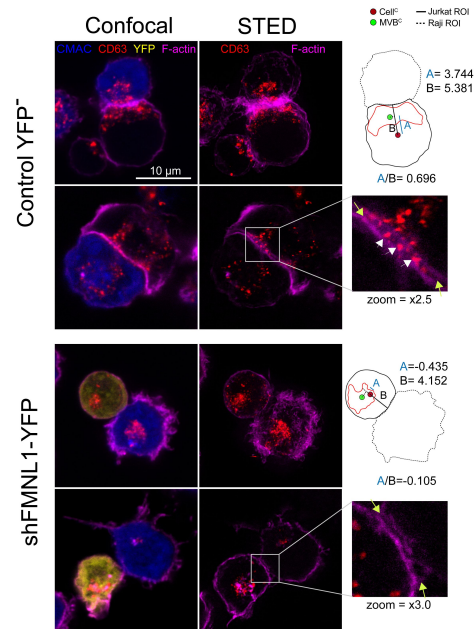


Fig. 10.

STED image of CD63⁺ nanovesicles at the synaptic cleft.

C3 control clone cells untransfected or expressing shFMNL1-HA-YFP were challenged with CMAC-labelled SEE-pulsed Raji cells (blue) for 1h, fixed, stained with phalloidinAF647 (magenta) and anti-CD63 (red) and imaged simultaneously by confocal and STED microscopy. Two representative control YFP⁻ and FMNL1-interfering (shFMNL1-HA-YFP) Jurkat cells forming IS with Raji cells are shown. Confocal (left) and STED (right) optical sections are shown, and enlarged (2.5 and 3X zoom) views of the IS areas are shown in the right side. The yellow arrows on the enlarged IS images label the edges of the synaptic cleft, which is the narrow, lane-shaped space between the two cells enclosed by the two F-actin-rich (magenta) plasma membrane leaflets. CD63⁺ MVB from the Jurkat cells are located nearby to the IS and some CD63⁺ nanovesicles (white arrows) are located at the synaptic cleft in the control YFP⁻ example. The diagrams used to calculate the MVB PI data in both cell groups are represented in the right side of the images. The zoom of the indicated ROIs (white square) is included below the diagrams. The percentage of synaptic conjugates on which was evident the presence of CD63⁺ nanovesicles at the synaptic cleft was 17% for control YFP⁻, and 0% for FMNL1-interfering (shFMNL1-HA-YFP), respectively, with at least 35 synapses analysed per condition. Images are representative of the data from several independent experiments (n=3) with similar results.

With regards to potential regulatory pathways involved in formin activation and subcellular localization, it is remarkable that the most abundant formins in T lymphocytes, Dia1 and FMNL1 (29), are constitutively inactive in the cytoplasm due to intramolecular DAD-DID binding, which blocks formin ability to nucleate and elongate actin filaments (7). Regarding a possible control of formin subcellular location by PKC, it has been shown that both relocation of FMNL2 from the plasma membrane to the endosomal compartment and activation are dependent on C-terminal S1072 phosphorylation by PKC α (32). However, FMNL2 location in filopodia seems to be independent of the phosphorylation state (33). We have previously described PKC δ -dependent phosphorylation of FMNL1 β (26), and here we have here demonstrated that this phosphorylation occurs at S1086, leading to F-actin reorganization at the IS, and resulting in MTOC polarization. However, in contrast to FMNL2 relocation, which is dependent on PKC α , we have shown that transient YFP-FMNL1 β WT relocation from cytosol to the IS occurred in the absence of PKC δ (Fig. 6), in conditions where neither F-actin reorganization (25) nor MTOC polarization (Fig. 5) occurred. Moreover, both YFP-FMNL1 β S1086A and YFP-FMNL1 β S1086D translocated to the IS (Suppl. Video 4 and Suppl. Fig. S8), demonstrating that S1086 phosphorylation is not required for IS location. However, as it happens during S1072 phosphorylation in FMNL2 (32), it is possible that blocking phosphorylation at S1086 through the introduction of single point mutations (YFP-FMNL1 β S1086A or YFP-FMNL1 β S1086D) may not block FMNL1 β translocation to the IS per se, but may alter the kinetics of the process. For this reason, in future approaches, a thorough study on the kinetic considerations on S1086 PKC δ -mediated phosphorylation contribution to FMNL1 β translocation to the IS will need to be addressed.

Jurkat T cells may not fully recapitulate the regulation of polarization in primary T cells, and the evidences from activating surfaces acting as artificial synapses show distinct actin cytoskeleton behavior (presence or not of F-actin foci) in primary versus immortalized T cells, at least in CD4⁺ cells, that may reflect mechanistic distinctions in the T-cell models systems utilized to study cytoskeletal actin dynamics (52) (53). However, to date, no clear evidence has been obtained regarding the existence of such an F-actin foci network in cell-cell immune synapse models based on primary T lymphocytes or Jurkat cells. F-actin foci have been exclusively observed in primary T cells engaged with artificial activating surfaces (planar lipid bilayers or coated glass), which does not apply to our data obtained from cell-cell synapses. However, to solve any potential differences in FMNL1 localization between primary versus immortalized T cells, we have performed experiments analyzing the subcellular localization of FMNL1 in CD19/CD22 dualtargeted CAR T cells forming synapses with CD19⁺/CD22⁺ Raji cells used as CTL targets and T lymphoblasts forming synapses with SEE and SEB-pulsed Raji cells. We observed, in fixed-cell images, the presence of endogenous FMNL1 colocalizing with F-actin-enriched areas in the IS region of both CAR T cells and primary T lymphoblasts, which also exhibited MTOC polarization towards the IS (Suppl. Fig. S7). The presence of FMNL1 at the IS developed by primary T lymphoblasts was transient, as occurred in Jurkat cells (not shown). These observations extend our results on FMNL1 localization at the IS in the Jurkat-Raji plus SEE synapse model to the IS developed by primary human T lymphocytes. Regarding exosome secretion in primary human T lymphocytes, additional experiments involving the expression of the diverse FMNL1 β variants will be necessary to assess whether FMNL1 β and its phosphorylation at S1086 controls exosome secretion in primary T lymphocytes, as occurred in Jurkat cells. These experiments will require the development of new transduction protocols to improve the otherwise inefficient expression in primary T lymphocytes, that it is even worse using the bicistronic large plasmids (>15 Kb) that we have employed in our studies. In addition, it is well known that the mere expression of large proteins such as the 180 kDa (30+150 kDa) YFP-FMNL1 chimeric variants constitutes a significant challenge. Thus, we have been unable to achieve enough transfection efficiency to perform these experiments, which would have allowed us to fully extend the effect of FMNL1 β and its phosphorylation at S1086 on exosome secretion to primary T cells. However, FMNL1 is necessary for MTOC/MVB polarization in Jurkat cells (29) (26), as confirmed in this manuscript, and this finding has already been extended to primary CD8⁺ T cell clones (29). All of this, together with the fact that exosome secretion requires MTOC/MVB polarization both in Jurkat cells and primary T lymphoblasts (2) (26),

suggests FMNL1 may also control exosome secretion in primary T cells, although the formal demonstration will require further research. Regarding the effect of the diverse FMNL1 β variants expression on MTOC/MVB polarization and exosome secretion in primary T lymphocytes, the data from activating surfaces clearly shows that the synaptic actin architecture of the IS from primary CD8⁺ T cells is essentially indistinguishable and thus unbiased from that of Jurkat T cells, but different to that of primary CD4⁺ cells (41 [DOI](#)). Thus, it is expected that all our data in Jurkat T cells could probably be extrapolated to the synaptic architecture of primary CD8⁺ cells, although more experiments involving primary CD4⁺ are necessary to extend all our results to the last cell type.

Although the mechanism(s) involved in FMNL1 β recruitment to the IS remains unclear, it is probably that it involves Rac1 and Cdc42 small G proteins (30 [DOI](#)) (29 [DOI](#)) (54 [DOI](#)), which are activated at the IS upon TCR triggering (55 [DOI](#)). However, we cannot exclude the participation of another PKC isoform or a different protein kinase that may induce FMNL1 β phosphorylation in different residues upon previous FMNL1 β relocation to the IS primed by small G protein, as was shown for FMNL2 relocation (32 [DOI](#)). Further experiments are needed to establish this important point.

Taken together, our results support that IS-induced, PKC δ -dependent phosphorylation of S1086 in FMNL1 β DAD, most probably executed by PKC δ itself, activates FMNL1 β , which in turn regulates cortical actin at the IS and hence controls MTOC/MVB polarization and exosome secretion. The behaviour of non-phosphorylatable YFP-FMNL1 β S1086A (equivalent to FMNL2-S1072A described in (32 [DOI](#))) confirms this hypothesis, since its expression inhibits F-actin reorganization at the IS, MTOC polarization and exosome secretion. In this respect, it has been reported that the phosphorylation of FMNL2 by PKC α in S1072 is necessary for the secretion of the prometastatic factor Angiopoietin-like 4 (ANGPTL4) in breast cancer cells (56 [DOI](#)), which constitutes the first description for an activated formin involvement in secretion during cell invasion. In addition, ANGPTL4 can be secreted into exosomes by lung cancer cells (57 [DOI](#)) (58 [DOI](#)) and FMNL2 controls exosome secretion (59 [DOI](#)). Thus, although it is not clear whether ANGPTL4 is released in exosomes or in soluble form (56 [DOI](#)), both FMNL2 and FMNL1 β appear to control PKC-regulated exosome secretion. However, the extracellular signals evoking exosome secretion are strikingly different in the various cell types, since in tumor cells hypoxia and radiation can amplify the otherwise constitutive and multidirectional exosome secretion, whereas T lymphocytes constitutively secrete very low levels of exosomes and none in a polarized manner unless activated through TCR or synaptic contact (22 [DOI](#)). Taken together, these considerations support a more general role of the formin-actin cytoskeleton axis in directional exosome secretion. Given all these considerations, it will be interesting to analyse the role of FMNL2 in inducible exosome secretion at the IS in T lymphocytes, but also the role of FMNL1 β in exosome secretion by cancer cells during cell invasion. This is particularly relevant as exosome secretion is required for directionally persistent and efficient *in vivo* movement of cancer cells (60 [DOI](#)), and it is known that FMNL1 stimulates both leukemia cell proliferation and migration (54 [DOI](#)) (61 [DOI](#)).

The fact that FMNL1- and PKC δ -interfered cells have a similar phenotype to that of FMNL1- or PKC δ -interfered cells (26 [DOI](#)) (25 [DOI](#)) (this paper), supports the notion that PKC δ and FMNL1 β participate in the same F-actin regulatory pathway controlling MTOC/MVB polarization. Additional experiments involving *in vitro* measurements of F-actin reorganizing/severing activities of the diverse FMNL1 β variants, phosphorylated or not *in vitro* by PKC δ , will be necessary to address whether PKC δ directly phosphorylates FMNL1 β at S1086.

Our findings show that FMNL1 colocalizes with F-actin at the IS edges which are part of the dSMAC (Figs. 6 [DOI](#), 8 [DOI](#)). This data are aligned with the previous observation that Dia1 and FMNL1 are intrinsically inactive because they undergo intramolecular folding and remain in the cytoplasm (7 [DOI](#)) and that after IS formation, they are enriched at the tips of F-actomyosin spikes at the outer edge of the dSMAC, giving rise to the actomyosin arcs at the pSMAC in the IS formed by Jurkat cells (41 [DOI](#)) (7 [DOI](#)). Dia1 is not a target of PKC, whereas FMNL1 is phosphorylated by PKC activation

(26 [↗](#)). Thus, in this paper we have focused on FMNL1. High resolution, spatio-temporal analysis of FMNL1 β localization at the different subsynaptic locations, together with superresolution techniques (41 [↗](#)) (43 [↗](#)) may provide new clues regarding the subsynaptic F-actin network targeted by phosphorylated FMNL1 β . Even although the nature of the downstream effectors and consequences of FMNL1 β phosphorylation on synaptic F-actin architecture can only be speculated at this point, concentric actomyosin arcs generated by FMNL1 propel TCR microclusters towards the IS and reinforce cytotoxicity (41 [↗](#)) (7 [↗](#)). Thus, high-resolution spatiotemporal analysis of actomyosin arcs structure and function during TCR microcluster movement in FMNL1-interfered cells, and/or cells expressing the FMNL1 β mutants described here, will provide important clues on this important matter. It is noteworthy that a majority of the image analysis of IS organization and F-actin dynamics is based on planar synapses obtained using artificial APC substitutes, by either coating stimulatory and co-stimulatory molecules on glass or plastic surfaces or by embedding these molecules into lipid bilayers (62 [↗](#)) (7 [↗](#)) (63 [↗](#)). These artificial synapses can indeed be imaged and analysed with the highest possible resolution (64 [↗](#)) (41 [↗](#)) (43 [↗](#)). However, the cell-cell synapse model analysed here mimics the complex interactions and irregular, 3D stimulatory surface of a physiological synapse better than artificial synapses do (62 [↗](#)) (7 [↗](#)). In this important sense, the data presented here are indeed closer to a physiological situation. In addition, since actomyosin arcs arise from active, formin-dependent nucleation sites at the outer edge of the dSMAC (41 [↗](#)), it will be interesting to analyse, using superresolution techniques, whether phosphorylated FMNL1 β is located at these sites. Indeed, actomyosin arc network spanning from dSMAC along the pSMAC is the most likely source of T cell-based force that augments cytotoxicity by straining the target cell plasma membrane (7 [↗](#)). Thus, it will be interesting to study the effect of FMNL1 β mutants on actomyosin arcs formation and analyse functional deficiencies (i.e., decreased T cell-APC adhesion frequency, IS size and IS formation efficiency) in IS formed by cells interfered in FMNL1 β and/or expressing the FMNL1 β variants described here. Visualization of actin and actomyosin networks, TCR microclusters and secretion granules dynamics in “real” live T cell-APC conjugates at the superresolution level (7 [↗](#)) is clearly needed to advance in this area.

Remarkably, although it has already been shown that FMNL1 is important for MTOC polarization in Jurkat cells and for target cell lysis in CTL (29 [↗](#)), our data provide the first molecular basis underpinning this essential FMNL1 function. Here, we demonstrate that FMNL1 β and its phosphorylation at S1086 participate in F-actin-controlled, polarized MVB traffic secreting effector exosomes in Jurkat T lymphocytes developing IS (2 [↗](#), 17 [↗](#)), which deliver proapoptotic signals to target cells (19 [↗](#)) (65 [↗](#)) (20 [↗](#)). In addition, FMNL1 promotes proliferation and migration of leukemia cells (54 [↗](#)) and mediates posterior perinuclear actin polymerization to promote T lymphocyte effector cell migration to inflammatory sites to enable T cell-mediated autoimmunity (61 [↗](#)). PKC δ is crucial for directional T cell migration (66 [↗](#)) (67 [↗](#)) and this process requires MVB polarized traffic and exosome secretion in the direction of migration (60 [↗](#)). For that reason, it will be interesting to analyse the effects of the FMNL1 β mutants we have described here during T lymphocyte migration and tumorigenesis, as well as to study the role of FMNL1 β phosphorylation in several autoimmune disorders. In addition, improving our understanding of the molecular bases underlying the traffic events involved in polarized secretion of pro-apoptotic exosomes as we have performed here, provided that the FMNL1 effect on exosome secretion in Jurkat cells can be extended to primary T lymphocytes, will deliver clues to modify crucial immune functions involving apoptosis, such as cytotoxicity by CTLs and immunoregulatory AICD and their associated pathologies. This may allow to design therapeutic strategies to modify CAR T lifespan and/or polarized secretory function, in order to improve their efficiency for the treatment of certain cancers (17 [↗](#)) (68 [↗](#)) (2 [↗](#)) (18 [↗](#)) (25 [↗](#)) (69 [↗](#)) (70 [↗](#)) (71 [↗](#)).

Materials and methods

Cells

Raji B cell line was obtained from the ATCC. Cell lines were cultured in RPMI 1640 medium containing L-glutamine (Invitrogen) with 10% heat-inactivated FCS (Gibco) and penicillin/streptomycin (Gibco). Jurkat control (C3 and C9) and PKC δ -interfered (P5 and P6) stable clones derived from JE6.1 clone have already been described and were cultured with puromycin (25 [25](#)). C3 and C9 control clones are used, instead of canonical JE6.1 cells, since these puromycin-resistant control clones (containing a scramble shRNA) were isolated by limiting dilution together with the PKC δ -interfered clones (25 [25](#)), thus are the best possible controls for P5 and P6 clones. The P5 and P6 clones exhibited a comparable defect in MVB/MTOC polarization when compared with the control clones (25 [25](#))(26 [26](#)). In addition, when interference-resistant GFP-PKC δ was transiently expressed in all the PKC δ interfered clones, MTOC/MVB polarization was recovered to control levels (25 [25](#)). Therefore, the deficient MTOC/MVB polarization in these clones is exclusively due to the reduction in PKC δ expression (25 [25](#)), and thus clonal variation cannot be responsible of the results in stable clones. Since the FMNL1 interference and YFP-FMNL1 variants re-expression experiments are performed in transient assays (2–4 days after transfection), there is no chance for any clonal variation in these short-time experiments. Peripheral mononuclear cells from healthy donors (La Paz University Hospital, Madrid, Spain) were stimulated with Phytohemagglutinin (PHA-M, 1 μ g/ml) for 3 days. Dual CAR T cells recognizing CD19/CD22 were produced as previously shown (72 [72](#)) and were provided by Department of Pediatric Hemato-Oncology, La Paz University Hospital (Madrid, Spain). Subsequently, both T lymphoblasts and CAR T cells were expanded in the presence of recombinant human IL-2 (20 ng/ml, Roche).

Plasmids and transient transfection

pEGFP-C1CD63 (expressing GFP-CD63) was provided by G. Griffiths. CD63 is an enriched marker in intraluminal vesicles (ILVs) contained into MVB and exosomes and has been widely used to study MVB secretory traffic in both living and fixed cells (2 [2](#), 17 [17](#)). The FMNL1 interfering vector (shFMNL1-HA-YFP) and FMNL1-interfering, YFP-FMNL1 β WT expressing vector (shFMNL1-HA-YFP-FMNL1 β WT) were previously described (35 [35](#)) and generously provided by Dr. Billadeau. shFMNL1-HA-YFP-FMNL1 β S1086A and shFMNL1-HA-YFP-FMNL1 β S1086D mutants were generated by site-directed mutagenesis, as previously reported (73 [73](#)). Briefly, overlap extension PCR was used to introduce the desired mutations into a 900 bp SalI-NotI fragment, which was then used to replace the corresponding wild type sequence in shFMNL1-HA-YFP-FMNL1 β -WT. All amplifications were carried out with Platinum SuperFi DNA polymerase (ThermoFisher). Primers used were: SalI-FMNL1 β _F (CCAGAGCCTGGATGCGCTGTGG), FMNL1 β -S1086A_F (CAGACACAGGCCGCGCTGCCGTCGGCGTCCC), FMNL1 β -S1086A_R (GGGACGCCGACGGCAGCGCGGCGCCTGTGTCTGC), FMNL1 β -S1086D_F (CAGACACAGGCCGCGGATGCCGTCGGCGTCCC), FMNL1 β -S1086D_R (GGGACGCCGACGGCATCGCGGCGCCTGTGTCTGC), and NotI-FMNL1 β _R (GCGAGCTCTAGGCGCCTTGCG). Presence of the desired mutations, and absence of undesired ones, was confirmed by Sanger DNA sequencing (Eurofins Genomics, LightRun). Both interference and expression of the different chimeric molecules were assessed in single cells level by immunofluorescence and/or bulk cell populations by WB with an anti-FMNL1 antibody, which recognizes all FMNL1 isoforms (see below). Jurkat clones were transiently transfected with 20–30 μ g of the plasmids as described (17 [17](#)). To analyse the effects of shFMNL1 constructs on exosome secretion by Jurkat cells expressing exosome reporter GFP-CD63, Jurkat cells were transiently co-transfected with a three-fold molar excess of the different shFMNL1-YFP plasmids with respect to the GFP-CD63 exosome-reporter plasmid, to favor that the exosomes analysed were mainly those secreted by Jurkat cells containing both the GFP-CD63 plasmid and the shFMNL1 construct (2 [2](#))(18 [18](#)).

Antibodies and reagents

Rabbit monoclonal anti-human PKC δ EP1486Y for WB that does not recognize mouse PKC δ (Abcam). Rabbit monoclonal anti-PKC δ EPR17075 for WB that recognizes both human and mouse PKC δ (Abcam). Mouse monoclonal anti-human CD3 (clone UCHT1) for cell stimulation and immunofluorescence (BD Biosciences and Santa Cruz Biotechnology). Mouse monoclonal anti-FMNL1 clone C-5 for WB and immunofluorescence and mouse monoclonal anti-FMNL1 clone A-4 for immunoprecipitation (Santa Cruz Biotechnology), recognizing all FMNL1 isoforms. Mouse monoclonal anti- γ -tubulin for immunofluorescence (SIGMA, clone GTU-88). Rabbit polyclonal anti-pericentrin ab4448 for immunofluorescence (Abcam). Mouse monoclonal anti-human CD63 (clone TEA3/18) for immunofluorescence (Immunostep). Mouse monoclonal anti-CD63 clone NKI-C-3 for WB (Oncogene). Rabbit polyclonal Phospho-Ser PKC substrate antibody for WB and immunofluorescence (Cell Signalling Technology, #2261). Fluorochrome-coupled secondary antibodies (goat-anti-mouse IgG AF488 A-11029, goat-anti-rabbit IgG AF488 A-11034, goat-anti-mouse IgG AF546 A-11030, goat-anti-mouse IgG AF647 A-21236) for immunofluorescence (ThermoFisher). Horseradish peroxidase (HRP)-coupled secondary antibodies (goat anti-mouse IgG-HRP, sc-2005 and goat anti-rabbit IgG-HRP, sc-2004) for WB (Santa Cruz Biotechnology). CellTracker™ Blue (CMAC) and phalloidin (ThermoFisher). Staphylococcal enterotoxin E (SEE) (Toxin Technology, Inc). Phytohemagglutinin (PHA-M) was from SIGMA. Recombinant human IL-2 was from Roche.

Immunoprecipitation

Immunoprecipitation from cell lysates was performed by using Protein A/G Magnetic Beads (Pierce, ThermoScientific) following the instructions provided by the company. Briefly, 0.5 ml lysates corresponding to $2\text{--}4 \times 10^6$ transfected Jurkat cells, stimulated or not with PMA (100 ng/ml, 30 min at 37 °C), were incubated with anti-FMNL1 (clone A4, 5 μ g) for 2 h at 4° C. Subsequently, 15 μ l of magnetic beads suspension was added and incubated for 3 h at 4° C. Beads were washed 5 \times with lysis buffer and the antigens were eluted with 2 M glycine pH =2 and then neutralized. Eluates were run on 6,5 % SDS-PAGE gels and proteins transferred to PVDF membranes.

Isolation and quantification of exosomes

To analyse the exosomes produced by cells transfected with the exosome reporter GFP-CD63, a similar protocol to the originally described for exosome isolation ([74](#)) was performed. We have included a 48 h post-transfection Ficoll gradient purification step to remove dead cells and cell debris, which otherwise could contaminate exosome preparations with micro and nanoparticles ([2](#), [18](#)). Using these standard protocols, culture supernatants from Jurkat cells transfected with GFP-CD63 or cotransfected with GFP-CD63 and with a 3-fold molar excess of the different shFMNL1-YFP plasmids, cocultured with SEE-pulsed Raji cells, were centrifuged in sequential steps to eliminate cells and cell debris/apoptotic bodies ([74](#)). Subsequently, the exosomes were recovered by ultracentrifugation (100,000 \times g for 12 h at 4° C) as described ([16](#)), lysed and then analysed by WB. CD63 is characteristically present in MVB, ILVs and hence in exosomes, but also in secretory lysosomes and the plasma membrane (Suppl. Video 8). Plasma membrane CD63 localization is produced by degranulation of MVB and diffusion of CD63 from the limiting membrane of MVB to the plasma membrane upon MVB fusion ([2](#), [18](#)) (Suppl. Video 8). Approximately $1\text{--}2 \times 10^6$ transfected Jurkat cells were challenged with SEE-pulsed Raji cells and WB signals in exosome lysates were normalized by the cell expression levels of GFP-CD63 among different transfections, cell groups and stimuli, in the WB corresponding to the cell lysates ([2](#), [47](#)) ([18](#)). It has been established that the exosomal CD63 WB signal in this synapse model correlates with exosome number obtained by flow cytometry ([75](#)), by electron microscopy ([76](#)) and by nanoparticle concentration analysis (nanoparticles/ml), using NTA ([18](#)). WB analysis of CD63 protein and GFP-tagged CD63 in isolated exosomes has been used as a *bona fide* method to specifically determine changes in exosome production ([17](#), [47](#), [77](#)) in

transiently-transfected Jurkat cells forming synapses with SEE-pulsed Raji cells without the detection of contaminating exosomes produced by MHC-II-stimulated Raji cells or constitutively secreted by Raji cells (78 [🔗](#)) (2 [🔗](#), 17 [🔗](#), 74 [🔗](#)) (18 [🔗](#)) (25 [🔗](#)) (22 [🔗](#)). No significant differences in the GFP-CD63 levels (i.e. **Fig. 9B** [🔗](#)) were observed in the lysates of transfected C3 Jurkat cells, stimulated or not with SEE-pulsed Raji cells, at the end of the cell coculture period for exosome secretion, showing that the GFP-CD63⁺ exosomes were produced by an equal number of viable, GFP-CD63-expressing cells. Moreover, to quantify exosome concentration and to analyse their size distribution, the cell culture supernatant collected just before the ultracentrifugation step was diluted (1/5) in Hank's balanced salt solution (HBSS) and analysed by NTA using a NANOSIGHT equipment (LM10, Malvern) that was calibrated with 50 nm, 100 nm and 400 nm fluorescent calibration beads (Malvern). The hydrodynamic diameter measured by NTA, although apparently higher to that originally described for exosomes using electron microscopy (50–100 nm) (**Fig. 9A** [🔗](#)), certainly corresponds to the real size of canonical, unfixed exosomes in solution, as described (79 [🔗](#)). The NTA measurements of exosome concentration (particles/ml) were normalized by the transfection efficiency and exosome-producing Jurkat cell number, by referring exosome concentration to GFP-CD63 signals in the WB of the cell lysates (**Fig. 9B** [🔗](#)).

Western blot analysis

Cells were lysed in TritonTM X100-containing lysis buffer supplemented with both protease and phosphatase inhibitors. Approximately 50 µg of cellular proteins were recovered in the 10,000xg pellet from 10⁶ cells. Cell lysates and neutralized, acid-eluted IPs were separated by SDS-PAGE under reducing conditions and transferred to HybondTM ECLTM membranes (GE Healthcare). Membranes were incubated sequentially with the different primary antibodies and developed with the appropriate HRP-conjugated secondary antibody using enhanced chemiluminescence (ECL). When required, blots were stripped following standard protocols prior to reprobing them with primary and HRP-conjugated secondary antibodies. For exosome secretion studies, cells and isolated exosomes were lysed in RIPA lysis buffer containing protease inhibitors. Approximately 5 µg of exosomal proteins were recovered in the 100,000xg pellet from 1–2×10⁶ cells. Exosomes were resuspended in 60 µl of RIPA lysis buffer and 20 µl of exosomal or cell lysate proteins were separated by SDS-PAGE and transferred to HybondTM ECLTM membranes (GE Healthcare). For CD63 detection, proteins were separated under non-reducing conditions as described (17 [🔗](#)). For WB analysis of exosomes, each lane contained the total exosomal protein that was recovered from the culture medium coming from the same number of cells, untreated or treated with stimuli. Blots were incubated with mouse anti-CD63 (clone NKI-C-3, Oncogene) and developed with the appropriate HRP-conjugated secondary antibody using ECL. Autoradiography films were scanned and the bands were quantified using Quantity One 4.4.0 (Bio-Rad) and ImageJ (Rasband, W.S., ImageJ, National Institutes of Health, Bethesda, Maryland, USA, <http://rsb.info.nih.gov/ij/> [🔗](#), 1997–2004) software.

Time-lapse microscopy, immunofluorescence and image analysis

In the experiments requiring IS formation, we challenged the transfected Jurkat clones with SEE-pulsed Raji cells, a well-established synapse model (80 [🔗](#)). Raji cells were attached either to ibiTreat microwell culture dishes (ibidi) pretreated with fibronectin (0.1 mg/ml, for paraformaldehyde-PFA-fixation) or glass bottom microwell culture dishes (ibidi) pretreated with poly-L-lysine (0.02 mg/ml, for PFA and acetone fixation). Next, they were labelled with CMAC (10 µM) and pulsed with 1 µg/ml SEE and mixed with Jurkat clones transfected with the different expression plasmids, at 24–48 h posttransfection. The resulting IS were analysed as described (80 [🔗](#)) (2 [🔗](#)) (44 [🔗](#)) (26 [🔗](#)). PFA followed by acetone fixation was required for a clean FMNL1 staining and was compatible with phalloidin labelling (81 [🔗](#)). Immunofluorescence of fixed synapses was performed as previously described (82 [🔗](#)), and additional blocking and fixations steps were performed between each primary antibody and subsequent fluorochrome-coupled secondary antibody or phalloidin staining, to exclude any potential cross-reaction of secondary antibodies (i.e., **Fig. 5** [🔗](#)).

For FMNL1 β relocation experiments in living cells, control (C3) and PKC δ -interfered (P5), YFP-FMNL1 β -expressing Jurkat clones were challenged with CMAC-labelled, SEE-pulsed Raji cells as described above. Wide-field, time-lapse microscopy was performed using an OKO-lab stage incubator (OKO) for sample ambient on a Nikon Eclipse TiE microscope equipped with a Prime BSI (Photometrics) digital camera, a PlanApo VC 60x/1.4NA OIL objective (Nikon) and with Perfect Focus System, allowing distinct, appropriate offsets per each XY field. Wide-field fluorescence of fixed synapses was performed by capturing 30–40 Z sections (0.3–0.4 μ m thickness) using the same microscope and NIS-AR software (Nikon), and maximum intensity projection (MIP) images of all channels were generated using NIS-AR software.

Time-lapse acquisition during the indicated times and analysis were performed using NIS-AR software (Nikon). Subsequently, in some experiments epifluorescence images were improved by Huygens Deconvolution Software from Scientific Volume Image, using the “widefield” optical option as previously described (43) (44). For quantification, digital images were analysed using NIS-AR (Nikon) or ImageJ software. The quantification and analysis of YFP MFI at the synapse area (YFP-FMNL1 β MFI IS) and at the whole cell (YFP-FMNL1 β MFI Cell) in time-lapse experiments, were performed within floating regions of interest (ROI) (i.e., ROI changing XY position over time) by using NIS-AR software (Fig. 6A and Suppl. Fig. S8).

Confocal microscopy imaging in fixed synapses was performed by using an SP8 Leica confocal microscope (63x/1.40 Oil DIC objective), with sequential acquisition, bidirectional scanning and the following laser lines: UV (405 nm, intensity: 33.4%), supercontinuum visible (633 nm, intensity: 15.2%), supercontinuum visible (550 nm, intensity: 20.8%), supercontinuum visible (488 nm, intensity: 31.2%). STED fluorescence microscopy was performed by using a Stellaris 8 Tau STED (Leica) equipped with a 775 nm depletion laser and a 100x/1.4 Oil STED white Objective. Deconvolution of confocal images and widefield images was performed by using Huygens Deconvolution Software from Scientific Volume Image with the “confocal” optical option or “widefield” option, respectively. 2D colocalization analyses were accomplished by using JACoP plugin from ImageJ, whereas interface colocalization and the corresponding videos to generate the IS interface were performed using the “colocalization” tool, followed by the “volume view” and then “movie maker” tools from NIS-AR. For interface colocalization analyses, the original emission colors of the different fluorochromes were changed to Red, Green or Blue, since NIS-AR requires and RGB color code for this analyses (83). In particular, F-actin and Phospho-Ser PKC substrate acquired in magenta were changed to blue, and YFP acquired in yellow was changed to green (i.e. Fig. 8, Suppl. Fig. S4, Suppl. Fig. S5 and Suppl. Fig. S11). Profile analyses of MFI corresponding to each separate channel and the colocalization pixels at the IS interface (ZX axes) were performed by using “Intensity Profile” tool in NIS-AR and then Excel, as reported (83). To measure the relative size of the F-actin low area at the cIS, which quantifies the decrease in F-actin density at the cIS, we used the last frame from the former IS interface videos (Suppl. Video 5 and Fig. 7), generated as described (83). The areas of the F-actin-low region at cIS (Fact-low cIS area) (yellow line) and the synapse (IS area) (white line) (i.e., Fig. 7) were defined in ImageJ using the ROI manager and applying an appropriate, manually-defined threshold to the F-actin channel. The definition of the ROI to measure the Fact-low cIS area and the IS area was performed manually or by using automated algorithm “auto-detect ROI/segmentation” from NISAR (25) (26). As for the Fact-low cIS area (yellow line) and the IS area (white line) (i.e., Fig. 7), they were defined in ImageJ using the ROI manager and applying a default threshold or, in cases where precise detection was not achieved, an appropriate, manually-defined threshold to the F-actin channel. In both cases, we have found that both manual and automated values were quite similar. The areas included in these ROIs were measured and limited to the defined thresholds, and the relative area of the F-actin-low region at the cIS (Fact-low cIS area / IS area), which is independent of both cell and synapse size, was calculated and represented (Fig. 7). Regarding the possibility that actin cytoskeleton of Raji cells can also contribute to the measurements of synaptic F-actin, it is important to remark that MHC-II-antigen triggering on the B cell side of the Th synapse does not induce noticeable F-actin changes along the synapse (i.e. F-actin clearing at the cIS), in contrast to

TCR stimulation on T cell side (84) (85) (3). In addition, we have observed that majority of F-actin at the IS belongs to the Jurkat cell (83). Thus, the contribution to the analyses of the residual, invariant F-actin from the B cell is negligible using our protocol (83).

To compare MTOC and MVB polarization in synapses, MTOC and MVB PI were calculated, as previously described (37) (25) (26) (86) (**Suppl. Fig. S2A**), using MIP, both for deconvoluted, wide-field, and confocal-acquired images. In the MIP, the positions of the cell geometric center ($Cell^C$) and MTOC and MVB center of mass ($MTOC^C$ and MVB^C , respectively) were used to project $MTOC^C$ (or MVB^C) on the vector defined by the $Cell^C$ -synapse axis. Then the MTOC (or MVB) PI was calculated by dividing the distance between the $MTOC^C$ (or MVB^C) projection and the $Cell^C$ ("B" or "A" distance, respectively) by the distance between the $Cell^C$ and the synapse ("C" distance) (**Suppl. Fig. S2A**, **Fig. 4** and **Fig. 5**). $Cell^C$ position was taken as the origin to measure distances, thus those "A" and "B" values in the opposite direction to the synapse were taken as negative. Thus, PI ($PI = A/C$ or B/C) ranked from +1 (fully polarized) to -1 (fully antipolarized). Therefore, PI values were normalized by cell size and shape (**Fig. 4**) (25) (86) and measured the relative ability of MTOC and MVB to polarize towards the IS. Remarkably, one important feature of the IS consists of both the onset of the initial cell-cell contacts and the establishment of a mature, fully productive IS, are intrinsically stochastic, rapid and asynchronous processes (87, 88) (43). Thus, the score of the PI corresponding to the distance of MTOC/MVB with respect the IS (42) may be contaminated by background MTOC/MVB polarization, in great part due to the stochastic nature of IS formation (87). In order to circumvent this caveat, a substantial number of IS of each cell group/condition were analysed to obtain statistically significant results, as reported by numerous authors (89) (37) (90) (87) (25) (26). Image analysis data correspond to at least three different experiments, analysing a minimum of 30 synapses from 15 different, randomly selected, microscopy fields per experiment. ANOVA was performed for statistical significance of the results using Excel and IBM's SPSS Statistics software.

Abbreviations:

- AICD: activation-induced cell death
- ANGPTL4: Angiopoietin-like 4
- APC: antigen-presenting cell
- BCR: B-cell receptor for antigen
- C: center of mass
- CAR T: chimeric antigen receptor-bearing T lymphocytes
- cIS: central region of the immune synapse
- CMAC: CellTracker™ Blue (7-amino-4-chloromethylcoumarin)
- cSMAC: central supramolecular activation cluster
- CTL: cytotoxic T lymphocytes
- DAD: diaphanous autoinhibitory domain
- Dia1: Diaphanous-1
- DID: diaphanous inhibitory domain
- dSMAC: distal supramolecular activation cluster
- ECL: enhanced chemiluminescence
- F-actin: filamentous actin
- Fact-low cIS: F-actin-low region at the center of the immune synapse
- FasL: Fas ligand
- FHOD1: formin homology domain protein 1
- FMNL1: formin-like 1
- fps: frames per second
- HBSS: Hank's balanced salt solution

- HRP: horseradish peroxidase
- ILVs: intraluminal vesicles
- IS: immune synapse
- IPs: immunoprecipitates
- MFI: mean fluorescence intensity
- MHC: major histocompatibility complex
- MIP: maximum intensity projection
- MVB: multivesicular bodies
- MTOC: microtubule-organizing center
- MW: molecular weight
- NTA: Nanoparticle Tracking Analyses
- NS: not significant
- PFA: paraformaldehyde
- PHA: Phytohemagglutinin
- PKC: protein kinase C
- PKC δ : protein kinase C δ
- PMA: phorbol myristate acetate
- PI: polarization index
- pSMAC: peripheral supramolecular activation cluster
- ROI: region of interest
- ROCK: Rho-dependent protein kinase
- SD: standard deviation
- SEE: *Staphylococcal* enterotoxin E
- SEB: *Staphylococcal* enterotoxin B
- SMAC: supramolecular activation cluster
- SMAPs: supramolecular attack particles
- TCR: T-cell receptor for antigen
- Th: T-helper
- TRANS: transmittance
- WB: western blot
- YFP: yellow fluorescent protein.

Acknowledgements

We are indebted and acknowledge Dr. D.D. Billadeau (Mayo Clinic, USA) for generous sharing of shFMNL1 and FMNL1 isoform rescue constructions. We acknowledge the excellent technical support from A. Sánchez. We acknowledge Dr. M.A. Alonso (CBM, CSIC) for reagents and scientific advice. We acknowledge the generous contribution of pre-graduate students Alejandro Martín, Irene Gascuña, Gregorio Pantoja, María Ruiz, Sofía Blázquez, Carlos del Hoyo, Pablo del Barrio and Elena Fernández to this work. Thanks to D. Morales (SIDI-UAM), A. Oña and G. D'Agostino (CNB, CSIC) and M. Martín (IIBM, CSIC) for their superb expertise with confocal microscopy. Work in the F.R.G-G lab was funded by grant PID2019-104941RB-I00 from the Spanish Ministry of Science and Innovation (MCIN/AEI/ 10.13039/501100011033). This work was supported by grants from the Programa Estatal de Investigación, Desarrollo e Innovación Orientada a los Retos de la Sociedad (Grant PID2020-114148RB-I00 from the Spanish Ministry of Science and Innovation MCIN/AEI/ 10.13039/501100011033) to MI.

Additional information

Conflict of Interest

The authors report no conflict of interest.

Author Contributions Statement

V.C. and M.I. conceived and designed all the experiments. J.R-N. did most of the experiments, analysed data, and contributed to the writing of the manuscript. J.R-N., S.F. and I.S. contributed to the MTOC/MVB polarization experiments and IS image analyses. S.F. and I.S. performed the FMNL1 immunoprecipitation experiments and contributed to the FMNL1 phosphorylation studies and image analyses, and J.R-N. contributed to timelapse studies and image analyses of area F-actin. A. N.-Z. and A. P.-M. developed the CART cells and CART synapses studies. P.B. and F.R.G.-G. created and sequenced the FMNL1 β mutants, and contributed to manuscript writing. M.I. conceptualized and coordinated the research, directed the study, analysed data, and wrote the manuscript. All the authors contributed to the planning and designing of the experiments and to helpful discussions.

Funding Statement

This work was supported by a grant from the Programa Estatal de Investigación, Desarrollo e Innovación, Modalidad Retos Investigación (Grant PID2020-114148RB-I00 funded by Spanish Ministry of Science and Innovation MCIN/AEI/ 10.13039/501100011033), and grant P2022/BMD-7225, funded by Consortia in Biomedicine of Comunidad de Madrid to M.I.

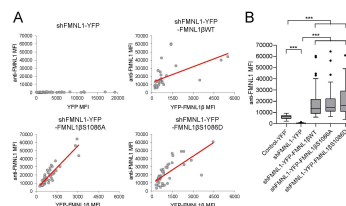
Data Availability Statement

The materials described in the manuscript, including all relevant raw data, will be freely available to any researcher wishing to use them for non-commercial purposes, without breaching participant confidentiality.

Additional Declarations:

The authors declare no competing interests.

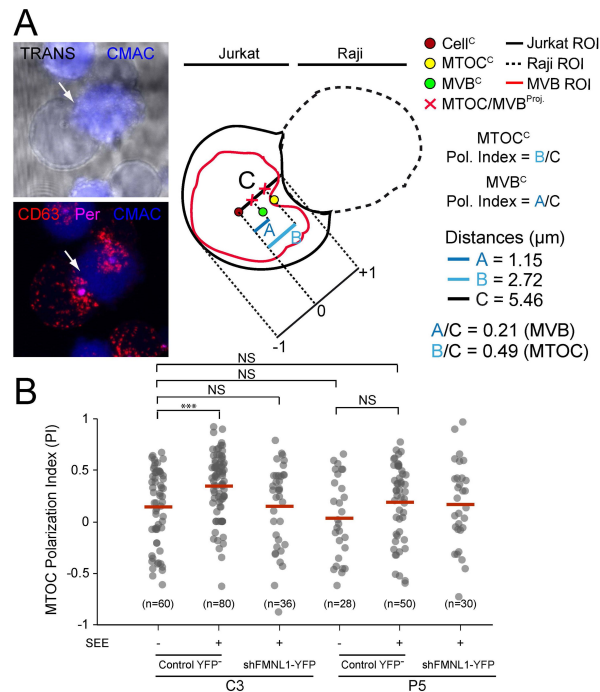
Supplementary figures



Supplementary Fig. S1.

Expression of YFP-FMNL1 β constructs and correlation between YFP-FMNL1 β variants expression and the anti-FMNL1 antibody signal.

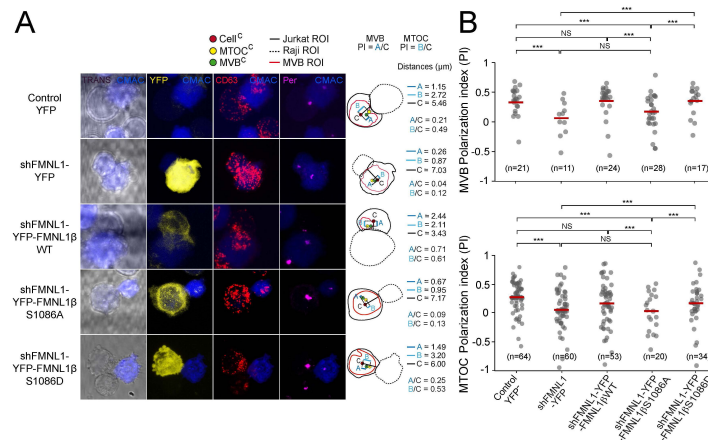
Panel A), Scatter plots of the MFI values of YFP or YFP-FMNL1 variants and the anti-FMNL1 signal in cells transfected with FMNL1-interfering (shFMNL1-HA-YFP), YFP-FMNL1 β WT (shFMNL1-HA-YFP-FMNL1 β WT), YFP-FMNL1 β S1086A, or YFP-FMNL1 β S1086D constructs are depicted. The trend line (linear regression) is displayed in red color in FMNL1 β constructions. Panel B), Box plot representing the different anti-FMNL1 MFI signals in the control and the different transfected cell groups. This figure is related to [Fig. 2](#). ***, $p \leq 0.05$. Results and ANOVA analyses are representative of the data from several independent experiments ($n=3$) with similar results.



Supplementary Fig. S2.

SEE-induced polarization of MVB and MTOC to the immune synapse and calculation of their polarization indexes.

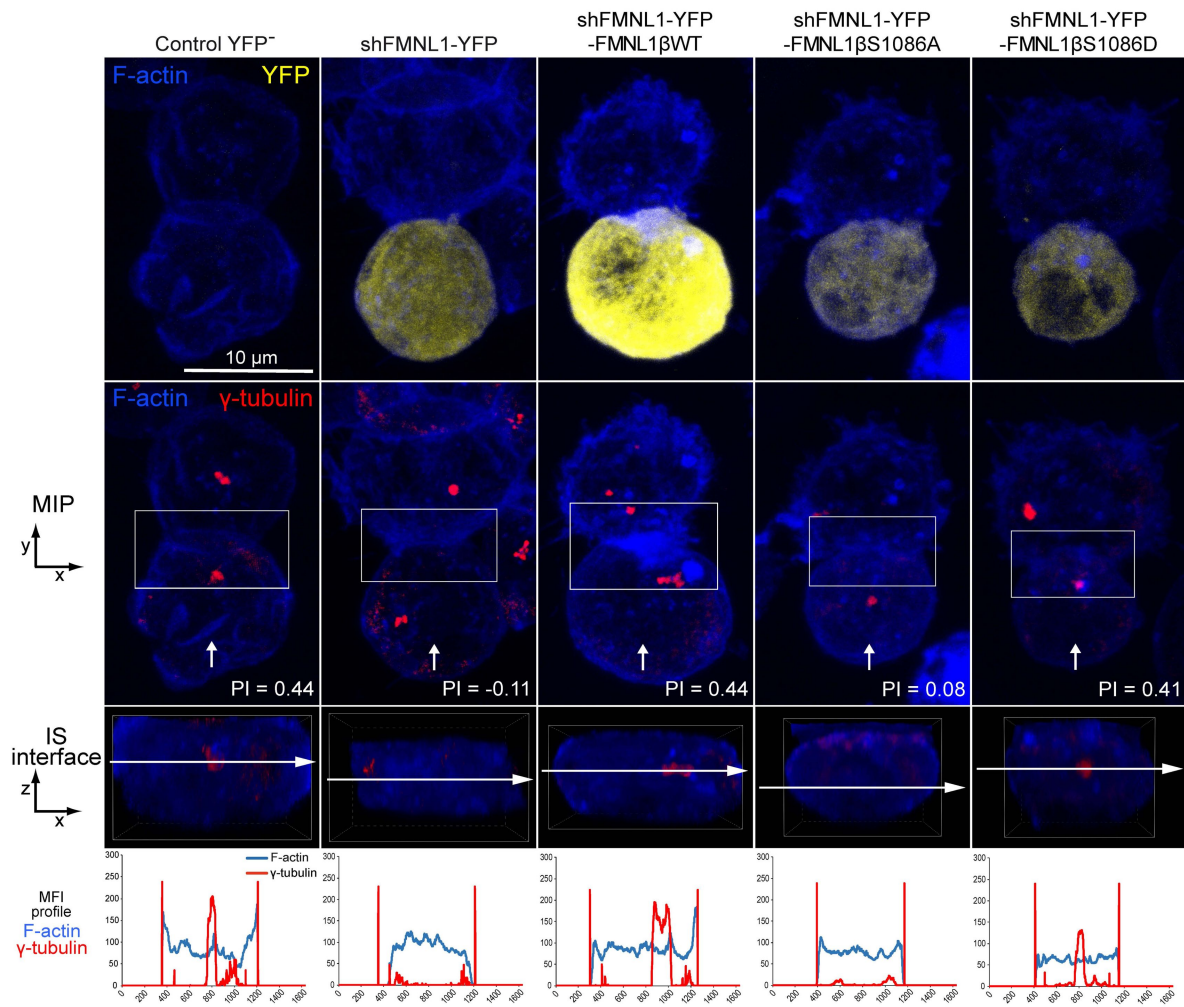
Panel A), In the left panels, synaptic cell conjugates made by Jurkat cells with CMAC-labeled, SEE-pulsed Raji cells (blue) were fixed, permeabilized and stained with anti-CD63 (red) and anti-pericentrin (magenta) antibodies to label MVB and the MTOC, respectively. The white arrow indicates the IS area. In the right-side scheme, the distances in color ("A", blue; "B", cyan and "C", black) used for the calculation of both MVB and MTOC PI (A/C and B/C, respectively) are indicated. The dark-red dot represents the cell geometric center (Cell^C), whereas the yellow and green dots indicates the MTOC and MVB center of mass (MTOC^C and MVB^C), respectively. The line "C" represents the distance between the Cell^C and the synapse, and the projections of both MTOC^C and MVB^C on the "C" line are labelled with red crosses (MTOC/MVB^{Proj}). Since the Cell^C position was taken as the origin to measure distances, those "A" or "B" values in the opposite direction to the synapse were taken as negative. Thus, PI ranged from +1 to -1. The Raji cells and the Jurkat clones are labelled with discontinuous and continuous white lines, respectively. Panel B), C3 control and PKCδ-interfered P5 clone were untransfected (Control YFP⁻) or transfected with FMNL1-interfering (shFMNL1-HA-YFP). Subsequently, cells were challenged with CMAC-labelled, unpulsed (SEE-) or SEE-pulsed (SEE+) Raji cells for 1 h, fixed, stained with anti-pericentrin (magenta) to label the MTOC and imaged by epifluorescence microscopy to measure MTOC PI as indicated in panel A. The dot plot shows the MTOC PI of each indicated cell group are shown. NS, not significant; ***, $p \leq 0.05$. Results and ANOVA analyses are representative of the data from several independent experiments (n=3) with similar results.



Supplementary Fig. S3.

FMNL1 β phosphorylation at S1086 is involved in MTOC / MVB polarization towards the immune synapse. Confocal analysis.

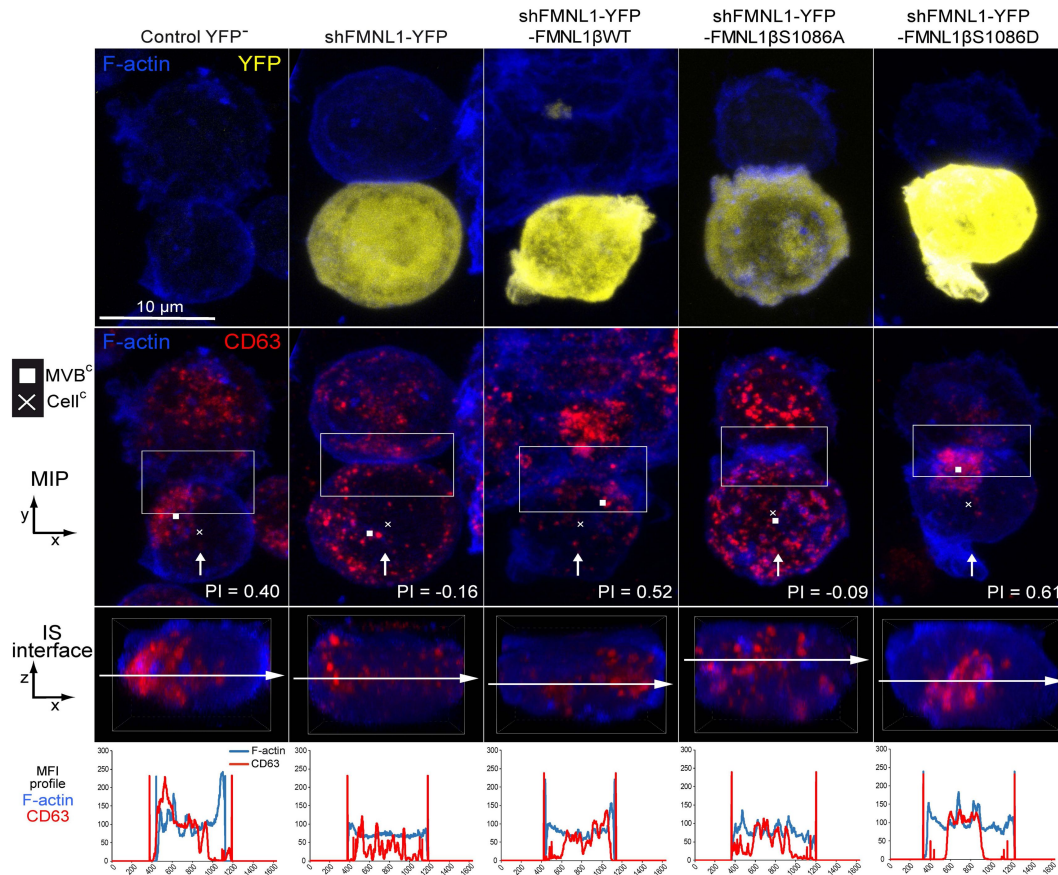
Untransfected, C3 clone (Control YFP⁻) (first row) and C3 clone transfected (yellow) with either FMNL1-interfering (shFMNL1-HA-YFP) (second row) or FMNL1-interfering and expressing interference-resistant YFP-FMNL1 β WT (shFMNL1-HA-YFP-FMNL1 β WT) (third row), or YFP-FMNL1 β S1086A (fourth row), or YFP-FMNL1 β S1086D (fifth row) constructs, were challenged with CMAC-labelled, SEEpulsed Raji cells (blue) for 1 h to form IS. Then, cell conjugates were fixed, stained with anti-pericentrin to label the MTOC (magenta) and anti-CD63 to label MVB (red), and imaged by confocal fluorescence microscopy. Panel A), representative MIP images with merged channels of each cell group specified in the left side, and the diagrams on the right represent the measurements of the parameters used to calculate the MTOC and MVB PI, including the distance between the IS and the center of the cell (Cell^C) and the IS (line C), the MTOC^C (line B) and the MVB^C (line A). Jurkat cell outlines are labelled with a continuous line, Raji cells are labelled with a dashed line, whereas ROI containing MVB are labelled with a continuous red line. Panel B), MTOC and MVB PI dot plot for the different cell groups corresponding to the indicated number of synapses from a similar experiment to that described in panel A) are represented. This figure is related to Fig. 4. NS, not significant. ***, $p \leq 0.05$. Results and ANOVA analyses are representative of the data from several independent experiments ($n=3$) with similar results.



Supplementary Fig. S4.

T cell *en face* analysis of F-actin and MTOC distribution at the immune synapse interface.

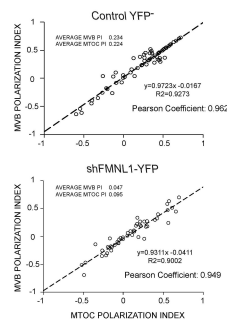
C3 control clone was untransfected (Control YFP⁻) (first column) or transfected with FMNL1-interfering (shFMNL1-HA-YFP) (second column), or FMNL1-interfering expressing interference-resistant YFP-FMNL1 β WT (shFMNL1-HA-YFP-FMNL1 β WT) (third column), YFP-FMNL1 β S1086A (fourth column), or YFP-FMNL1 β S1086D (fifth column) constructs. Subsequently, cells were challenged with CMAC-labelled SEE-pulsed Raji cells (blue) for 1 h, fixed, stained with phalloidin (magenta) and anti- γ -tubulin (red). The corresponding shFMNL1 constructions are in yellow, and cells were imaged by confocal fluorescence microscopy. Please realize that F-actin (acquired in magenta) was changed to blue color. The upper row includes the top, yx views corresponding to the MIP images of representative examples of each transfected cell group. In the second row, the same examples are displayed, showing the relative MTOC position of each transfected cell group and MTOC PI is indicated in white types. Vertical white arrows indicate the direction to visualize the *en face* views of the IS (IS interface) enclosed by the ROIs (white rectangles), as shown in [Suppl. Video 1](#). Subsequently, in the third row the *en face* zx views were generated by merging the indicated channels in the second row of each panel (F-actin in blue merged to anti- γ -tubulin in red), on the IS interfaces of the synaptic areas (generated as shown in [Suppl. Video 1](#)). The last frame of this video corresponds to *en face* view (interface) (third row). MFI profiles along the indicated line (horizontal white arrow) of each separate channel (F-actin in blue, anti- γ -tubulin in red) are shown below the IS interfaces. This figure is related to [Fig. 4](#) and [7](#). Results are representative of data from several independent experiments (n=3) with similar results.



Supplementary Fig. S5.

T cell *en face* analysis of F-actin and MVB distribution at the immune synapse interface.

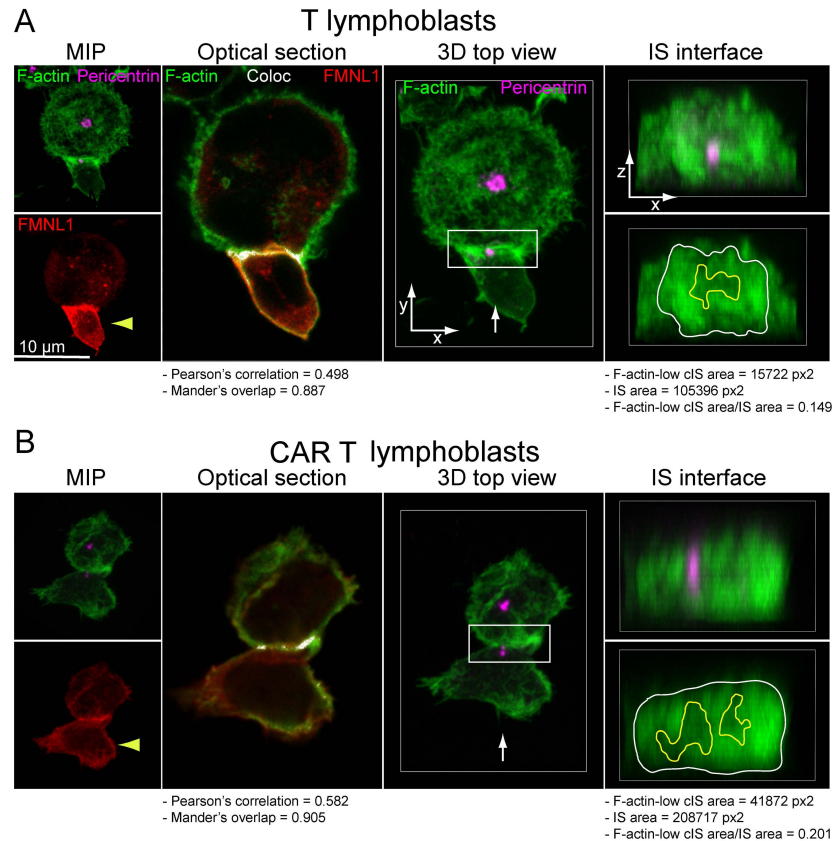
C3 control clone was untransfected (Control YFP⁻) (first column) or transfected with FMNL1-interfering (shFMNL1-HA-YFP) (second column), or FMNL1-interfering expressing interference-resistant YFP-FMNL1βWT (shFMNL1-HA-YFP-FMNL1βWT) (third column), YFP-FMNL1βS1086A (fourth column), or YFP-FMNL1βS1086D (fifth column) constructs. Subsequently, cells were challenged with CMAC-labelled SEE-pulsed Raji cells (blue) for 1 h, fixed, stained with phalloidin (magenta) and anti-CD63 (red). The corresponding shFMNL1 constructions are in yellow, and cell conjugates were imaged by confocal fluorescence microscopy. Please realize that F-actin (acquired in magenta) was changed to blue color. The upper row includes the top, yx views corresponding to the MIP images of representative examples of each transfected cell group. In the second row, the same examples are displayed, showing the MVB position in each transfected cell group and MVB PI is indicated in white types. Vertical white arrows indicate the direction to visualize the *en face* views of the IS (IS interface) enclosed by the ROIs (white rectangles), as shown in [Suppl. Video 2](#). The white cross represents the position of the geometric center of the Jurkat cell (Cell^C), while the white square represents the position of the center of mass of the distribution of MVB (MVB^C) that it is an unbiased parameter that mirrors MVB center of mass polarization. Subsequently, in the third row, the *en face* zx views were generated by merging the indicated channels in the second row of each panel (F-actin in blue merged to anti-CD63 in red), on the IS interfaces of the synaptic areas (generated as shown in [Suppl. Video 2](#)). The last frame of these videos corresponds to *en face* views (interface) (third row). MFI profiles along the indicated line (horizontal white arrow) of each separate channel (F-actin in blue, anti-CD63 in red) are shown below the IS interfaces. When MVB are not polarized, some MVB can still be observed at cIS because they are scattered throughout the cell. For instance, the YFP-FMNL1βWT transfected cell (third column) shows a pronounced MVB concentration within the synaptic area (white rectangle), whereas the YFP-FMNL1βS1086A transfected cell (fourth column), as it presents a scattered distribution of MVB throughout the cell, also exhibits some MVB (but only a small proportion of the total cellular MVB) in the synaptic area (second row). This figure is related to [Fig. 4](#) and [7](#). Results are representative of the data from several independent experiments (n=3) with similar results.



Supplementary Fig. S6.

Correlation between MTOC and MVB polarization indexes.

C3 control untransfected (Control YFP⁻) and C3 transfected with the FMNL1-interfering plasmid (shFMNL1-HA-YFP) were challenged with CMAC-labelled SEE-pulsed Raji cells for 1 h, fixed, stained with anti- γ -tubulin AF647 to label MTOC and anti-CD63 AF546, to label MVB and imaged by confocal fluorescence microscopy. Subsequently, MTOC and MVB PI were calculated for the synapses established by both cell groups, as described in Materials and Methods and shown in schematic representation in **Suppl. Fig. S2A**. Linear correlation analyses between the MTOC and MVB PI for both cell groups are represented, as well as the corresponding linear correlation analysis data and the Pearson's coefficients. Dashed lines represent the adjusted, regression line. This figure is related to **Fig. 4**. Results are representative of data from several independent experiments (n=3) with similar results.



Supplementary Fig. S7.

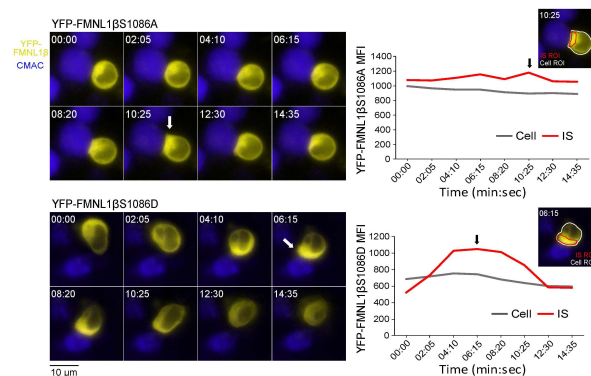
FMNL1 is located at the immune synapse developed by primary T lymphoblasts and dual CAR T cells recognizing CD19/CD22.

Primary T lymphoblasts and dual CAR T cells recognizing CD19/CD22 growing in the presence of recombinant human IL-2 cells were challenged with SEE plus SEB-pulsed Raji cells for 30 min (panel A), or Raji cells for 1 h (panel B), respectively. After the indicated coculture times, cell conjugates were fixed, and stained with phalloidinAF488 (green), anti-pericentrin (magenta) and anti-FMNL1 (red). Synapses were imaged with confocal fluorescence microscopy and colocalization pixels between FMNL1 (red) and F-actin (green) are represented in white (Coloc). Representative MIP and optical sections of synapses formed by both cell types are shown in the left side columns. The effector T lymphocytes are labelled with a yellow arrow in these figures. The F-actin/FMNL1 colocalization coefficients measured in the IS ROI are indicated in the second column. In the right-side columns, top views and IS interface views of the IS are included, as well as the F-actin IS interface architecture and MTOC position. The multifocal nature of the synapse developed by CAR T cells (71 [Fig. 6](#) and [Fig. 8](#)) is evident. This figure is related to [Fig. 6](#) and [Fig. 8](#). The percentage of synapse conjugates substantiating endogenous FMNL1 at the IS was 15% for lymphoblasts and 12% for CAR T, respectively, with at least 120 synapses analysed per condition. Results are representative of data from several independent experiments (n=3) with similar results.

Supplementary Fig. S8.

YFP-FMNL1 β S1086A and S1086D mutants are recruited to the immune synapse.

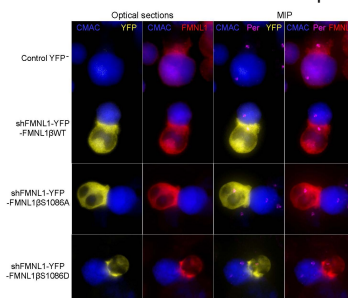
C3 control cells were transfected with FMNL1-interfering expressing interference-resistant YFP-FMNL1 β S1086A or S1086D (shFMNL1-HA-YFP-FMNL1 β S1086A or shFMNL1-HA-YFP-FMNL1 β S1086D) plasmids. Subsequently, transfected cells were simultaneously challenged with CMAC-labelled, SEE-pulsed Raji cells (blue) attached to slides and time-lapse acquisition of emerging synapses was performed as indicated in Materials and Methods. The videos (7 fps) (Suppl. Video 4) were captured and in the left side, representative frames from each video are shown. White arrows indicate accumulations of YFP-FMNL1 β S1086A or S1086D at the IS. In the right side, YFP-FMNL1 β S1086A or S1086D MFI within the cell ROI (grey line) and the IS ROI (red line) are represented. The inserts in the diagrams include the cell ROI (white) and the IS ROI (red) used for the time-lapse measurements on representative frames for both FMNL1 β mutants. This figure is related to Fig. 6 and Suppl. Video 4. At least 6 synapses of each cell group were analysed. Results are representative of data from several independent experiments (n=3) with similar results.

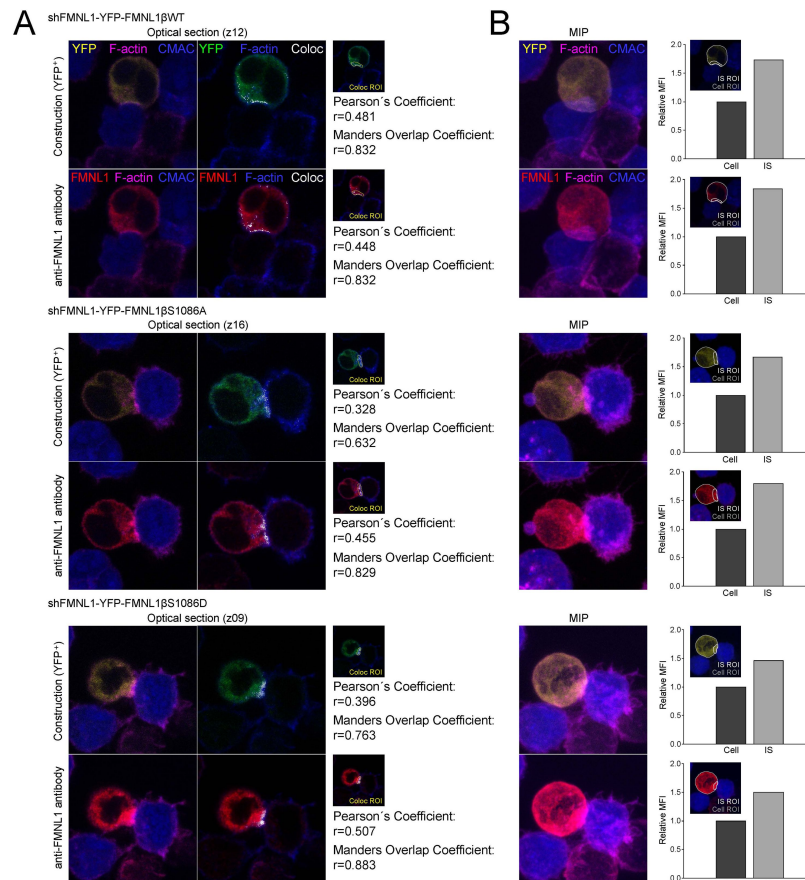


Supplementary Fig. S9.

FMNL1 and FMNL1 β accumulation at the immune synapse revealed by epifluorescence microscopy.

C3 control clone was untransfected (Control YFP⁻) (first row) or transfected with FMNL1-interfering expressing interference-resistant YFP-FMNL1 β WT (shFMNL1-HA-YFP-FMNL1 β WT) (second row) or YFP-FMNL1 β S1086A (third row) or YFP-FMNL1 β S1086D (fourth row) constructs. Subsequently, cells were challenged with CMAC-labelled SEE-pulsed Raji cells (blue) for 1 h, fixed, stained with anti-pericentrin (magenta) and anti-FMNL1 (red) and imaged by epifluorescence microscopy. The corresponding FMNL1 β constructions are in yellow, whose signal is observed in both the first and third columns. The first and second columns represent those individual optical sections in which the accumulation of FMNL1 or FMNL1 β variant in the IS formed by each cell group is better visualized, while the third and fourth columns represent MIPs of the same selected cells. FMNL1 or FMNL1 β variant accumulation at the IS can be visualized in red or yellow, respectively. This figure is related to Fig. 6. Results are representative of the data from several independent experiments (n=3) with similar results.

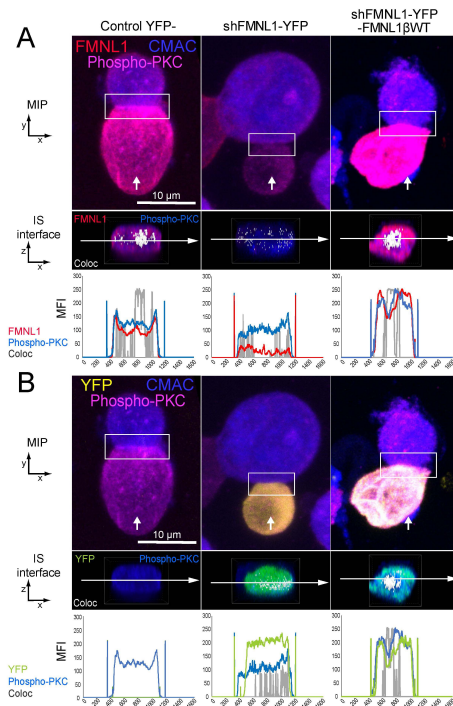




Supplementary Fig. S10.

YFP-FMNL1β variants accumulation at the immune synapse revealed by confocal fluorescence microscopy.

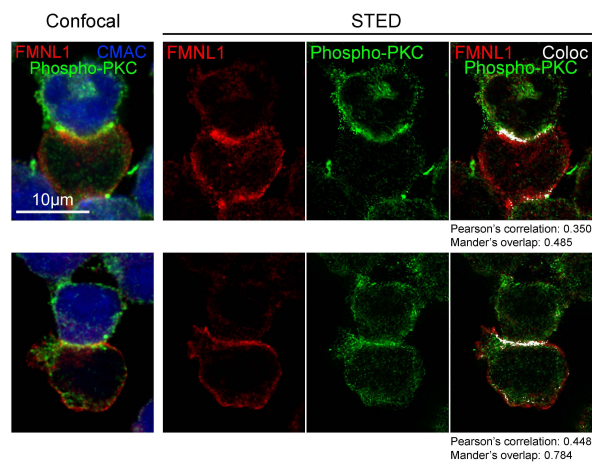
C3 control clone was transfected with FMNL1-interfering expressing interferenceresistant YFP-FMNL1βWT (shFMNL1-HA-YFP-FMNL1βWT) (first and second rows), YFP-FMNL1βS1086A (third and fourth rows) or YFP-FMNL1βS1086D (fifth and sixth rows) constructs. Subsequently, cells were challenged with CMAC-labelled SEE-pulsed Raji cells (blue) for 1 h, fixed, stained with phalloidin (magenta) and anti-FMNL1 (red). The corresponding shFMNL1 constructions are in yellow, and cells were imaged by confocal fluorescence microscopy. Panel A), top views corresponding to representative examples of each transfected cell group are shown. The first column includes those individual optical sections in which the accumulation of each FMNL1β variant in the IS formed by each cell group is better visualized. Please realize that, since colocalization in NIS-AR only works with red, green and blue channels, F-actin (acquired in magenta) was changed to blue color, and YFP (acquired in yellow) was changed to green in the second column of each panel, where colocalization pixels between anti-FMNL1 or YFP-FMNL1β and F-actin in the same optical section are shown in white. The third column displays the ROIs used to measure the indicated colocalization coefficients. The Pearson and Manders colocalization coefficients for each of the selected cells are displayed. Panel B), the MIPs of the same cells displayed in panel A) are shown. At the right side, the relative MFI quantification of the accumulation at the IS of YFP-FMNL1β variants and FMNL1 compared to the signal of the entire cell is shown. This figure is related to [Fig. 6](#). Results are representative of data from several independent experiments (n=3) with similar results.



Supplementary Fig. S11.

Colocalization of FMNL1 and anti-phospho-Ser PKC substrate at the immune synapse interface.

Untransfected, control C3 clone (Control YFP⁻) (first column) and C3 clone transfected with either FMNL1-interfering (shFMNL1-HA-YFP) (second column), or FMNL1-interfering and expressing interference-resistant YFP-FMNL1βWT (shFMNL1-HA-YFP-FMNL1βWT) (third column) constructs were challenged with CMAC-labelled SEE-pulsed Raji cells (blue) for 1 h, fixed, stained with anti-Phospho-Ser PKC substrate (magenta) and anti-FMNL1 (red), and imaged by confocal fluorescence microscopy. Please realize that interface colocalization in NIS-AR only works with red, green and blue channels, therefore anti-Phospho-Ser PKC substrate (acquired in magenta) was changed to blue color, and YFP (acquired in yellow) was changed to green, for this purpose. Panel A), The upper row includes representative examples of the top yx views corresponding to the MIP images of the indicated, merged channels of each cell group. The white arrows indicate the direction to visualize the *en face* zx views of the IS (IS interface) enclosed by the ROIs (white rectangles), as shown in **Suppl. Video 7**. In the second row, the enlarged ROIs (2x zoom) used to generate the IS interface images of each cell group are shown. Subsequently, the colocalization pixels (white) along all the Z stacks were generated by merging the indicated channels in the second row of each panel (anti-phospho-Ser PKC substrate in blue merged to anti-FMNL1 in red), on the IS interfaces of the synaptic areas (generated as shown in **Suppl. Video 7**). The last frame of this video corresponded to *en face* view (interface) (second row on each panel). MFI profile along the indicated line (horizontal white arrow) of each separate channel (anti-phospho-Ser PKC substrate in blue and anti-FMNL1 in red) and the colocalization pixels (grey) are shown below the IS interfaces. Panel B), same as panel A), but both the top views and the IS interfaces were generated and stained with anti-phospho-Ser PKC substrate (blue) merged to YFP (green). At least 8 synapses of each cell group were analysed. Results are representative of data from several independent experiments (n=3) with similar results.



Supplementary Fig. S12.

STED colocalization of FMNL1 and anti-phospho-Ser PKC substrate at the immune synapse.

Control C3 clone was challenged with CMAC-labelled SEE-pulsed Raji cells (blue) for 1 h, fixed, stained with anti-Phospho-Ser PKC substrate (magenta) and anti-FMNL1 (red), and imaged by confocal and STED fluorescence microscopy and two representative examples are shown. Please realize that colocalization in NIS-AR only works with red, green and blue channels, therefore anti-Phospho-Ser PKC substrate (acquired in magenta) was changed to green color, and FMNL1 maintains red color. Subsequently, the colocalization pixels (white) along an optical section were generated by merging the indicated channels in the fourth column of each example (anti-phospho-Ser PKC substrate in green merged to anti-FMNL1 in red). In both cases, colocalization is specifically detected in the synaptic zone. First column, confocal Images. Right columns, STED colocalization. The FMNL1/Phospho-PKC colocalization coefficients are indicated in the right-side column. This figure is related to **Suppl. Fig. S11**. Results are representative of data from several independent experiments (n=3) with similar results.

Supplementary Fig. S13.

P-values from tukey's method (post hoc).

P-values after applying tukey's method to the indicated pairwise comparisons from the indicated figures are indicated

P-VALUES AFTER APPLYING TUKEY'S METHOD
(POST HOC) TO THE ONE-WAY ANOVA

Fig. 4

MITOC PI

Control vs. shFMSL1 (0.0411)
Control vs. FMSL1JPWT (0.7609)
Control vs. FMSL1JPS1086A (0.0011)
Control vs. FMSL1JPS1086D (0.0071)
shFMSL1 vs. FMSL1JPWT (0.4620)
shFMSL1 vs. FMSL1JPS1086A (0.0044)
shFMSL1 vs. FMSL1JPS1086D (0.0221)
FMSL1JPWT vs. FMSL1JPS1086A (0.2526)
FMSL1JPWT vs. FMSL1JPS1086D (0.5426)
FMSL1JPS1086A vs. FMSL1JPS1086D (0.0014)

MITOC PI

Control vs. shFMSL1 (0.0316)
Control vs. FMSL1JPWT (0.4793)
Control vs. FMSL1JPS1086A (0.0062)
Control vs. FMSL1JPS1086D (0.0079)
shFMSL1 vs. FMSL1JPWT (0.3793)
shFMSL1 vs. FMSL1JPS1086A (0.0099)
shFMSL1 vs. FMSL1JPS1086D (0.1077)
FMSL1JPWT vs. FMSL1JPS1086A (0.2890)
FMSL1JPWT vs. FMSL1JPS1086D (0.0757)
FMSL1JPS1086A vs. FMSL1JPS1086D (0.0054)

Fig. 5

(P5) Control vs. shFMSL1 (0.0099)
(P5) Control vs. FMSL1JPWT (0.0994)
(P5) Control vs. FMSL1JPS1086A (0.0099)

(P5) Control vs. FMSL1JPS1086D (0.0061)
(P5) Control vs. Control (C3) (0.1057)
(P5) Control vs. shFMSL1 (C3) (0.1813)
(P5) shFMSL1 (C3) vs. FMSL1JPWT (0.0044)
(P5) shFMSL1 (C3) vs. FMSL1JPS1086A (0.0098)
(P5) shFMSL1 (C3) vs. FMSL1JPS1086D (0.0088)
(P5) shFMSL1 (C3) vs. Control (C3) (0.1715)
(P5) shFMSL1 (C3) vs. shFMSL1 (C3) (0.0001)
(P5) FMSL1JPWT vs. FMSL1JPS1086A (0.0099)
(P5) FMSL1JPWT vs. FMSL1JPS1086D (0.0099)
(P5) FMSL1JPWT vs. Control (C3) (0.0496)
(P5) FMSL1JPWT vs. shFMSL1 (C3) (0.0071)
(P5) FMSL1JPS1086A vs. shFMSL1 (C3) (0.0079)
(P5) FMSL1JPS1086A vs. Control (C3) (0.0079)
(P5) FMSL1JPS1086D vs. shFMSL1 (C3) (0.0088)
(P5) FMSL1JPS1086D vs. Control (C3) (0.0090)
(P5) FMSL1JPS1086D vs. shFMSL1 (C3) (0.0478)
(P5) Control vs. shFMSL1 (C3) (0.0089)

Fig. 7

Control vs. shFMSL1 (0.0001)
Control vs. FMSL1JPWT (0.001)
Control vs. FMSL1JPS1086A (0.0075)
Control vs. FMSL1JPS1086D (0.001)
shFMSL1 vs. FMSL1JPWT (0.001)
shFMSL1 vs. FMSL1JPS1086A (0.0001)
shFMSL1 vs. FMSL1JPS1086D (0.001)
FMSL1JPWT vs. FMSL1JPS1086A (0.001)
FMSL1JPWT vs. FMSL1JPS1086D (0.001)
FMSL1JPS1086A vs. FMSL1JPS1086D (0.0001)
Suppl. Fig. S2

Control vs. FMSL1JPWT (0.0001)
Control vs. FMSL1JPS1086A (0.0001)
Control vs. FMSL1JPS1086D (0.0001)
shFMSL1 vs. FMSL1JPWT (0.0001)
shFMSL1 vs. FMSL1JPS1086A (0.0001)
shFMSL1 vs. FMSL1JPS1086D (0.0001)
FMSL1JPWT vs. FMSL1JPS1086A (0.7496)
FMSL1JPWT vs. FMSL1JPS1086D (0.0138)
FMSL1JPS1086A vs. FMSL1JPS1086D (0.2089)

Suppl. Fig. S2

Control (C3) vs. Control (C3) no SEE (0.0176)
Control (C3) vs. shFMSL1 (C3) (0.1057)
Control (C3) vs. Control (P5) (0.1813)
Control (C3) vs. Control (P5) no SEE (0.0021)
Control (C3) vs. shFMSL1 (P5) (0.2056)
Control (C3) vs. SEE vs. shFMSL1 (C3) (0.0099)
Control (C3) vs. SEE vs. Control (P5) (0.0050)
Control (C3) vs. SEE vs. Control (P5) no SEE (0.7075)
Control (C3) vs. SEE vs. shFMSL1 (P5) (0.9998)
shFMSL1 (C3) vs. Control (P5) (0.9979)
shFMSL1 (C3) vs. Control (P5) no SEE (0.7907)
shFMSL1 (C3) vs. shFMSL1 (P5) (0.9999)
Control (P5) vs. Control (P5) no SEE (0.4793)
Control (P5) vs. shFMSL1 (P5) (0.9997)
Control (P5) vs. SEE vs. shFMSL1 (P5) (0.7572)

Suppl. Fig. S3

MITOC PI

Control vs. shFMSL1 (0.0005)
Control vs. FMSL1JPWT (0.1210)
Control vs. FMSL1JPS1086A (0.0126)
Control vs. FMSL1JPS1086D (0.6577)
shFMSL1 vs. FMSL1JPWT (0.5356)

MEK1L1 vs. FAK1, Q10H8A (0.007)
MEK1L1 vs. FAK1, Q10H8D (0.017)
FUS1, Q1P7 vs. FAK1, Q10H8A (0.009)
FUS1, Q1P7 vs. FAK1, Q10H8D (0.007)
FUS1, Q10H8A vs. FAK1, Q10H8D (0.000)
MMP1
Control vs. MEK1L1 (0.002)
Control vs. FAK1, Q1P7 (0.000)
Control vs. FAK1, Q10H8A (0.000)
Control vs. FAK1, Q10H8D (0.000)
MEK1L1 vs. FAK1, Q1P7 (0.000)
MEK1L1 vs. FAK1, Q10H8A (0.000)
MEK1L1 vs. FAK1, Q10H8D (0.000)
FUS1, Q1P7 vs. FAK1, Q10H8A (0.000)
FUS1, Q1P7 vs. FAK1, Q10H8D (0.000)
FUS1, Q10H8A vs. FAK1, Q10H8D (0.000)

Supplementary Fig. S13. (continued)

References

1. Dustin ML, Choudhuri K (2016) **Signaling and Polarized Communication Across the T Cell Immunological Synapse** *Annu Rev Cell Dev Biol* **32**:303–25
2. Alonso R, Mazzeo C, Rodriguez MC, Marsh M, Fraile-Ramos A, Calvo V, et al. (2011) **Diacylglycerol kinase alpha regulates the formation and polarisation of mature multivesicular bodies involved in the secretion of Fas ligand-containing exosomes in T lymphocytes** *Cell death and differentiation* **18**:1161–73
3. Calvo V, Izquierdo M (2021) **Role of Actin Cytoskeleton Reorganization in Polarized Secretory Traffic at the Immunological Synapse** *Frontiers in cell and developmental biology* **9**
4. de la Roche M, Asano Y, Griffiths GM (2016) **Origins of the cytolytic synapse** *Nature reviews Immunology* **16**:421–32
5. Huse M (2012) **Microtubule-organizing center polarity and the immunological synapse: protein kinase C and beyond** *Frontiers in immunology* **3**
6. Monks CR, Freiberg BA, Kupfer H, Sciaky N, Kupfer A (1998) **Three-dimensional segregation of supramolecular activation clusters in T cells** *Nature* **395**:82–6
7. Hammer JA, Wang JC, Saeed M, Pedrosa AT (2018) **Origin, Organization, Dynamics, and Function of Actin and Actomyosin Networks at the T Cell Immunological Synapse** *Annu Rev Immunol* **37**:201–24
8. Blumenthal D, Burkhardt JK (2020) **Multiple actin networks coordinate mechanotransduction at the immunological synapse** *The Journal of cell biology* **219**
9. Ritter AT, Angus KL, Griffiths GM (2013) **The role of the cytoskeleton at the immunological synapse** *Immunological reviews* **256**:107–17
10. Billadeau DD, Nolz JC, Gomez TS (2007) **Regulation of T-cell activation by the cytoskeleton** *Nature reviews Immunology* **7**:131–43
11. Griffiths GM, Tsun A, Stinchcombe JC (2010) **The immunological synapse: a focal point for endocytosis and exocytosis** *The Journal of cell biology* **189**:399–406
12. Ritter AT, Asano Y, Stinchcombe JC, Dieckmann NM, Chen BC, Gawden-Bone C, et al. (2015) **Actin depletion initiates events leading to granule secretion at the immunological synapse** *Immunity* **42**:864–76
13. Chemin K, Bohineust A, Dogniaux S, Turret M, Guegan S, Miro F, et al. (2012) **Cytokine secretion by CD4+ T cells at the immunological synapse requires Cdc42-dependent local actin remodeling but not microtubule organizing center polarity** *Journal of immunology* **189**:2159–68
14. Peters PJ, Geuze HJ, Van der Donk HA, Slot JW, Griffith JM, Stam NJ, et al. (1989) **Molecules relevant for T cell-target cell interaction are present in cytolytic granules of human T lymphocytes** *European journal of immunology* **19**:1469–75

15. Peters PJ, Borst J, Oorschot V, Fukuda M, Krahenbuhl O, Tschopp J, et al. (1991) **Cytotoxic T lymphocyte granules are secretory lysosomes, containing both perforin and granzymes** *J Exp Med* **173**:1099–109
16. Martinez-Lorenzo MJ, Anel A, Gamen S, Monle n I, Lasiererra P, Larrad L, et al. (1999) **Activated human T cells release bioactive Fas ligand and APO2 ligand in microvesicles** *Journal of immunology* **163**:1274–81
17. Alonso R, Rodriguez MC, Pindado J, Merino E, Merida I, Izquierdo M (2005) **Diacylglycerol kinase alpha regulates the secretion of lethal exosomes bearing Fas ligand during activation-induced cell death of T lymphocytes** *The Journal of biological chemistry* **280**:28439–50
18. Mazzeo C, Calvo V, Alonso R, Merida I, Izquierdo M (2016) **Protein kinase D1/2 is involved in the maturation of multivesicular bodies and secretion of exosomes in T and B lymphocytes** *Cell death and differentiation* **23**:99–109
19. Bálint Š, Müller S, Fischer R, Kessler BM, Harkiolaki M, Valitutti S, et al. (2020) **Supramolecular attack particles are autonomous killing entities released from cytotoxic T cells** *Science* :897–901
20. Cassioli C, Baldari CT (2022) **The Expanding Arsenal of Cytotoxic T Cells** *Frontiers in immunology* **13**
21. Monleon I, Martinez-Lorenzo MJ, Monteagudo L, Lasiererra P, Taules M, Iturralde M, et al. (2001) **Differential secretion of Fas ligand- or APO2 ligand/TNF-related apoptosisinducing ligand-carrying microvesicles during activation-induced death of human T cells** *Journal of immunology* **167**:6736–44
22. Calvo V, Izquierdo M (2020) **Inducible Polarized Secretion of Exosomes in T and B Lymphocytes** *International Journal of Molecular Sciences* **21**
23. Krammer PH, Arnold R, Lavrik IN (2007) **Life and death in peripheral T cells** *Nature reviews Immunology* **7**:532–42
24. Nagata S, Suda T (1995) **Fas and Fas ligand: lpr and gld mutations** *Immunology today* **16**:39–43
25. Herranz G, Aguilera P, Davila S, Sanchez A, Stancu B, Gomez J, et al. (2019) **Protein Kinase C delta Regulates the Depletion of Actin at the Immunological Synapse Required for Polarized Exosome Secretion by T Cells** *Frontiers in immunology* **10**
26. Bello-Gamboa A, Velasco M, Moreno S, Herranz G, Ilie R, Huetos S, et al. (2020) **Actin reorganization at the centrosomal area and the immune synapse regulates polarized secretory traffic of multivesicular bodies in T lymphocytes** *J Extracell Vesicles* **9**
27. Ma JS, Haydar TF, Radoja S (2008) **Protein kinase C delta localizes to secretory lysosomes in CD8+ CTL and directly mediates TCR signals leading to granule exocytosis-mediated cytotoxicity** *Journal of immunology* **181**:4716–22
28. Ma JS, Monu N, Shen DT, Mecklenbrauker I, Radoja N, Haydar TF, et al. (2007) **Protein kinase Cdelta regulates antigen receptor-induced lytic granule polarization in mouse CD8+ CTL** *Journal of immunology* **178**:7814–21

29. Gomez TS, Kumar K, Medeiros RB, Shimizu Y, Leibson PJ, Billadeau Daniel D (2007) **Formins Regulate the Actin-Related Protein 2/3 Complex-Independent Polarization of the Centrosome to the Immunological Synapse** *Immunity* **26**:177–90
30. Kühn S, Geyer M (2014) **Formins as effector proteins of Rho GTPases** *Small GTPases* **5**
31. Kumari S, Curado S, Mayya V, Dustin ML (2014) **T cell antigen receptor activation and actin cytoskeleton remodeling** *Biochimica et biophysica acta* **1838** <https://doi.org/10.1016/j.bbamem.2013.05.004>
32. Wang Y, Arjonen A, Pouwels J, Ta H, Pausch P, Bange G, et al. (2015) **Formin-like 2 Promotes β 1-Integrin Trafficking and Invasive Motility Downstream of PKC α** *Developmental Cell* **34**:475–83
33. Lorenzen L, Frank D, Schwan C, Grosse R (2023) **Spatiotemporal Regulation of FMNL2 by N-Terminal Myristoylation and C-Terminal Phosphorylation Drives Rapid Filopodia Formation** *Biomolecules* **13**
34. Trefzer R, Elpeleg O, Gabrusskaya T, Stepensky P, Mor-Shaked H, Grosse R, et al. (2021) **Characterization of a L136P mutation in Formin-like 2 (FMNL2) from a patient with chronic inflammatory bowel disease** *PLOS ONE* **16**
35. Colon-Franco JM, Gomez TS, Billadeau DD (2011) **Dynamic remodeling of the actin cytoskeleton by FMNL1 γ is required for structural maintenance of the Golgi complex** *J Cell Sci* **124**:3118–26
36. Han Y, Eppinger E, Schuster IG, Weigand LU, Liang X, Kremmer E, et al. (2009) **Formin-like 1 (FMNL1) is regulated by N-terminal myristoylation and induces polarized membrane blebbing** *The Journal of biological chemistry* **284**:33409–17
37. Obino D, Diaz J, Saez JJ, Ibanez-Vega J, Saez PJ, Alamo M, et al. (2017) **Vamp-7-dependent secretion at the immune synapse regulates antigen extraction and presentation in B-lymphocytes** *Mol Biol Cell* **28**:890–7
38. Bertrand F, Muller S, Roh KH, Laurent C, Dupre L, Valitutti S (2013) **An initial and rapid step of lytic granule secretion precedes microtubule organizing center polarization at the cytotoxic T lymphocyte/target cell synapse** *Proc Natl Acad Sci U S A* **110**:6073–8
39. Nath S, Christian L, Tan SY, Ki S, Ehrlich LIR, Poenie M (2016) **Dynein Separately Partners with NDE1 and Dynactin To Orchestrate T Cell Focused Secretion** *The Journal of Immunology* **197**:2090–101
40. Ueda H, Zhou J, Xie J, Davis MM (2015) **Distinct Roles of Cytoskeletal Components in Immunological Synapse Formation and Directed Secretion** *Journal of immunology* **195**:4117–25
41. Murugesan S, Hong J, Yi J, Li D, Beach JR, Shao L, et al. (2016) **Formin-generated actomyosin arcs propel T cell receptor microcluster movement at the immune synapse** *The Journal of cell biology* **215**:383–99
42. Kupfer A, Singer SJ (1989) **Cell biology of cytotoxic and helper T cell functions: immunofluorescence microscopic studies of single cells and cell couples** *Annu Rev Immunol* **7**:309–37

43. Calvo V, Izquierdo M (2018) **Imaging Polarized Secretory Traffic at the Immune Synapse in Living T Lymphocytes** *Frontiers in immunology* **9**
44. Bello-Gamboa A, Izquierdo JM, Velasco M, Moreno S, Garrido A, Meyers L, et al. (2019) **Imaging the Human Immunological Synapse** *Journal of visualized experiments : JoVE*
45. Le Floc'h A, Huse M (2015) **Molecular mechanisms and functional implications of polarized actin remodeling at the T cell immunological synapse** *Cell Mol Life Sci* **72**:537–56
46. Thery C, Ostrowski M, Segura E (2009) **Membrane vesicles as conveyors of immune responses** *Nature reviews Immunology* **9**:581–93
47. Trajkovic K, Hsu C, Chiantia S, Rajendran L, Wenzel D, Wieland F, et al. (2008) **Ceramide triggers budding of exosome vesicles into multivesicular endosomes** *Science* :1244–7
48. Schönichen A, Geyer M (2010) **Fifteen formins for an actin filament: a molecular view on the regulation of human formins** *Biochim Biophys Acta* **1803**:152–63
49. Takeya R, Taniguchi K, Narumiya S, Sumimoto H (2008) **The mammalian formin FHOD1 is activated through phosphorylation by ROCK and mediates thrombin-induced stress fibre formation in endothelial cells** *EMBO J* **27**:618–28
50. Zhou Q, Wei SS, Wang H, Wang Q, Li W, Li G, et al. (1979) **Crucial Role of ROCK2-Mediated Phosphorylation and Upregulation of FHOD3 in the Pathogenesis of Angiotensin II-Induced Cardiac Hypertrophy** *Hypertension* :1070–83
51. Nishikawa K, Toker A, Johannes FJ, Songyang Z, Cantley LC (1997) **Determination of the specific substrate sequence motifs of protein kinase C isozymes** *The Journal of biological chemistry* **272**:952–60
52. Kumari S, Colin-York H, Irvine DJ, Fritzsche M (2019) **Not All T Cell Synapses Are Built the Same Way** *Trends Immunol* **40**:977–80
53. Colin-York H, Kumari S, Barbieri L, Cords L, Fritzsche M (2019) **Distinct actin cytoskeleton behaviour in primary and immortalised T-cells** *J Cell Sci* **133**
54. Favaro P, Traina F, Machado-Neto JA, Lazarini M, Lopes MR, Pereira JK, et al. (2013) **FMNL1 promotes proliferation and migration of leukemia cells** *Journal of leukocyte biology* **94**:503–12
55. Deckert M, Moon C, Le Bras S, Boquet P, Lemichez E (2005) **The Immunological Synapse and Rho GTPases** *Bacterial Virulence Factors and Rho GTPases* :61–90
56. Frank D, Moussi CJ, Ulferts S, Lorenzen L, Schwan C, Grosse R (2023) **Vesicle-Associated Actin Assembly by Formins Promotes TGFβ-Induced ANGPTL4 Trafficking, Secretion and Cell Invasion** *Advanced Science* **10**
57. Fang M, Yanwu X, Junling Z, Lin Z, Chen W, Xiaofei C, et al. (2020) **Effects of Hypoxia and Radiation-Induced Exosomes on Migration of Lung Cancer Cells and Angiogenesis of Umbilical Vein Endothelial Cells** *Radiation Research* **194**:71–80
58. Zhang Y, Liu X, Zeng L, Zhao X, Chen Q, Pan Y, et al. (2022) **Exosomal protein angiopoietin-like 4 mediated radioresistance of lung cancer by inhibiting ferroptosis under hypoxic microenvironment** *British Journal of Cancer* **127**:1760–72

59. He G, Li W, Zhao W, Men H, Chen Q, Hu J, et al. (2023) **Formin-like 2 promotes angiogenesis and metastasis of colorectal cancer by regulating the EGFL6/CKAP4/ERK axis** *Cancer Science* **114**:2014–28
60. Sung BH, Ketova T, Hoshino D, Zijlstra A, Weaver AM (2015) **Directional cell movement through tissues is controlled by exosome secretion** *Nature communications* **6**
61. Thompson SB, Sandor AM, Lui V, Chung JW, Waldman MM, Long RA, et al. (2020) **Formin-like 1 mediates effector T cell trafficking to inflammatory sites to enable T cell-mediated autoimmunity** *eLife* **9**
62. Dustin ML (2009) **Supported bilayers at the vanguard of immune cell activation studies** *J Struct Biol* **168**:152–60
63. Dupré L, Boztug K, Pfajfer L (2021) **Actin Dynamics at the T Cell Synapse as Revealed by Immune-Related Actinopathies** *Frontiers in cell and developmental biology* **9**
64. Carisey AF, Mace EM, Saeed MB, Davis DM, Orange JS (2018) **Nanoscale Dynamism of Actin Enables Secretory Function in Cytolytic Cells** *Curr Biol* **28**:489–502
65. Chang HF, Schirra C, Ninov M, Hahn U, Ravichandran K, Krause E, et al. (2022) **Identification of distinct cytotoxic granules as the origin of supramolecular attack particles in T lymphocytes** *Nature communications* **13**
66. Fanning A, Volkov Y, Freeley M, Kelleher D, Long A (2005) **CD44 cross-linking induces protein kinase C-regulated migration of human T lymphocytes** *International immunology* **17**:449–58
67. Volkov Y, Long A, Kelleher D (1998) **Inside the crawling T cell: leukocyte function-associated antigen-1 cross-linking is associated with microtubule-directed translocation of protein kinase C isoenzymes beta(I) and delta** *Journal of immunology* **161**:6487–95
68. Alonso R, Mazzeo C, Merida I, Izquierdo M (2007) **A new role of diacylglycerol kinase alpha on the secretion of lethal exosomes bearing Fas ligand during activation-induced cell death of T lymphocytes** *Biochimie* **89**:213–21
69. Stinchcombe J, Bossi G, Griffiths GM (2004) **Linking albinism and immunity: the secrets of secretory lysosomes** *Science* :55–9
70. de Saint Basile G, Menasche G, Fischer A (2010) **Molecular mechanisms of biogenesis and exocytosis of cytotoxic granules** *Nature reviews Immunology* **10**:568–79
71. Davenport AJ, Cross RS, Watson KA, Liao Y, Shi W, Prince HM, et al. (2018) **Chimeric antigen receptor T cells form nonclassical and potent immune synapses driving rapid cytotoxicity** *Proc Natl Acad Sci U S A* **115**
72. Ibáñez-Navarro M, Fernández A, Escudero A, Estes G, Campos-Silva C, Navarro-Aguadero MÁ, et al. (2023) **NKG2D-CAR memory T cells target pediatric T-cell acute lymphoblastic leukemia in vitro and in vivo but fail to eliminate leukemia initiating cells** *Frontiers in immunology* **14**
73. Barbeito P, Tachibana Y, Martin-Morales R, Moreno P, Mykytyn K, Kobayashi T, et al. (2021) **HTR6 and SSTR3 ciliary targeting relies on both IC3 loops and C-terminal tails** *Life Science Alliance* **4**

74. Thery C, Amigorena S, Raposo G, Clayton A (2006) **Isolation and characterization of exosomes from cell culture supernatants and biological fluids** *Current protocols in cell biology / editorial board, Juan S Bonifacino [et al]*
75. Ostrowski M, Carmo NB, Krumeich S, Fanget I, Raposo G, Savina A, et al. (2010) **Rab27a and Rab27b control different steps of the exosome secretion pathway** *Nature cell biology* **12**:19–30
76. Ventimiglia LN, Fernandez-Martin L, Martinez-Alonso E, Anton OM, Guerra M, Martinez-Menarguez JA, et al. (2015) **Cutting Edge: Regulation of Exosome Secretion by the Integral MAL Protein in T Cells** *Journal of immunology* **195**:810–4
77. Raiborg C, Rusten TE, Stenmark H (2003) **Protein sorting into multivesicular endosomes** *Current opinion in cell biology* **15**:446–55
78. Muntasell A, Berger AC, Roche PA (2007) **T cell-induced secretion of MHC class II-peptide complexes on B cell exosomes** *EMBO J* **26**:4263–72
79. Skliar M, Chernyshev VS, Belnap DM, Sergey GV, Al-Hakami SM, Bernard PS, et al. (2018) **Membrane proteins significantly restrict exosome mobility** *Biochem Biophys Res Commun* **501**:1055–9
80. Montoya MC, Sancho D, Bonello G, Collette Y, Langlet C, He HT, et al. (2002) **Role of ICAM-3 in the initial interaction of T lymphocytes and APCs** *Nat Immunol* **3**:159–68
81. Abrahamsen G, Sundvold-Gjerstad V, Habtamu M, Bogen B, Spurkland A (2018) **Polarity of CD4+ T cells towards the antigen presenting cell is regulated by the Lck adapter TSAAd** *Sci Rep* **8**
82. Jambriña E, Alonso R, Alcalde M, del Carmen Rodríguez M, Serrano A, Martínez AC, et al. (2003) **Calcium influx through receptor-operated channel induces mitochondria-triggered paraptotic cell death** *The Journal of biological chemistry* **278**:14134–45
83. Ruiz-Navarro J, Blázquez-Cucharero S, Calvo V, Izquierdo M (2023) **Imaging the immune synapse: three-dimensional analysis of the immune synapse** *Methods in cell biology*
84. Na BR, Kwon MS, Chae MW, Kim HR, Kim CH, Jun CD, et al. (2016) **Transgelin-2 in B-Cells Controls T-Cell Activation by Stabilizing T Cell - B Cell Conjugates** *PLoS One* **11**
85. Yuseff MI, Pierobon P, Reversat A, Lennon-Dumenil AM (2013) **How B cells capture, process and present antigens: a crucial role for cell polarity** *Nature reviews Immunology* **13**:475–86
86. Fernández-Hermira S, Sanz-Fernández I, Botas M, Calvo V, Izquierdo M (2023) **Analysis of centrosomal area actin reorganization and centrosome polarization upon lymphocyte activation at the immunological synapse** *Methods in cell biology* **173**:15–32
87. Yi J, Wu X, Chung AH, Chen JK, Kapoor TM, Hammer JA (2013) **Centrosome repositioning in T cells is biphasic and driven by microtubule end-on capture-shrinkage** *The Journal of cell biology* **202**:779–92
88. Friedl P, den Boer AT, Gunzer M (2005) **Tuning immune responses: diversity and adaptation of the immunological synapse** *Nature reviews Immunology* **5**:532–45

89. Duchez S, Rodrigues M, Bertrand F, Valitutti S (2011) **Reciprocal polarization of T and B cells at the immunological synapse** *Journal of immunology* **187**:4571–80
90. Obino D, Farina F, Malbec O, Saez PJ, Maurin M, Gaillard J, et al. (2016) **Actin nucleation at the centrosome controls lymphocyte polarity** *Nature communications* **7**

Editors

Reviewing Editor

Felix Campelo

Institute of Photonic Sciences, Barcelona, Spain

Senior Editor

Felix Campelo

Institute of Photonic Sciences, Barcelona, Spain

Joint Public Review:

Summary

Based on i) the documented role of FMNL1 proteins in IS formation; ii) their ability to regulate F-actin dynamics; iii) the implication of PKCdelta in MVB polarization to the IS and FMNL1beta phosphorylation; and iv) the homology of the C-terminal DAD domain of FMNL1beta with FMNL2, where a phosphorylatable serine residue regulating its auto-inhibitory function had been previously identified, the authors have addressed the role of S1086 in the FMNL1beta DAD domain in F-actin dynamics, MVB polarization and exosome secretion, and investigated the potential implication of PKCdelta, which they had previously shown to regulate these processes, in FMNL1beta S1086 phosphorylation. They demonstrate that FMNL1beta is indeed phosphorylated on S1086 in a PKCdelta-dependent manner and that S1086-phosphorylated FMNL1beta acts downstream of PKCdelta to regulate centrosome and MVB polarization to the IS and exosome release. They provide evidence that FMNL1beta accumulates at the IS where it promotes F-actin clearance from the IS center, thus allowing for MVB secretion.

Strengths

The work is based on a solid rationale, which includes previous findings by the authors establishing a link between PKCdelta, FMNL1beta phosphorylation, synaptic F-actin clearance and MVB polarization to the IS. The authors have thoroughly addressed the working hypotheses using robust tools. Among these, of particular value is an expression vector that allows for simultaneous RNAi-based knockdown of the endogenous protein of interest (here all FMNL1 isoforms) and expression of wild-type or mutated versions of the protein as YFP-tagged proteins to facilitate imaging studies. The imaging analyses, which are the core of the manuscript, have been complemented by immunoblot and immunoprecipitation studies, as well as by the measurement of exosome release (using a transfected MVB/exosome reporter to discriminate exosomes secreted by T cells).

Weaknesses

As stated in the title of the article, the main findings have been obtained in clones of Jurkat cells and have not been confirmed in primary T cells.

<https://doi.org/10.7554/eLife.96942.3.sa1>

Author response:

The following is the authors' response to the previous reviews.

eLife Assessment

This is a valuable study in the Jurkat T cell line that calls attention to phosphorylation of formin-like 1 β role and its role in polarization of CD63 positive extracellular vesicles (referred to as exosomes). The evidence presented in the Jurkat model is solid, but concerns have been raised about the statistical analysis and more details would be required to fully assess the significance of the results. For example, ANOVA is the method described, but it requires large amounts of normally distributed data in multiple groups and cannot be used to make pairwise comparisons within groups, which would require a post-hoc method (which is not discussed). In addition, the data showing forming-like 1 β in primary human T cells without and with a CAR are provided without quantification and don't investigate any of the novel claims, so doesn't address the relevance of Formin-like 1 β beyond the Jurkat model. Nonetheless, the consistent trends in the body of the study provide solid support for the claims.

We acknowledge this general statement on statistics. Thus, we have now discussed and provided more details on the post-hoc method (Tukey), as a new Supplementary data S13 (p-values after applying tukey's method -post hoc- to the one-way anova for all the pairwise comparisons). Additionally, we have now provided quantitative data on the percentage of primary cells with and without CAR that show FMNL1 accumulations at the immune synapse (Suppl. Fig. S7). Regarding the data in primary human T cells, we have already changed the title of the manuscript to strictly adjust it to the main body of the data and our conclusions in the well-established Jurkat synapse model. We also want to emphasize that we have not pretended to extrapolate the relevance of our data regarding FMNL1 and exosomes beyond the Jurkat model. Thus, we have included some additional sentences and/or nuances in the Discussion to somewhat soften our statements in this regard (i.e. “.....provided that the FMNL1 effect on exosome secretion in Jurkat cells can be extended to primary T lymphocytes”) and to clarify this important point.

Reviewer 1:

(1) The main findings have been obtained in clones of Jurkat cells. They have not been confirmed in primary T cells. The only experiment performed in primary cells is shown in Figure S7 (primary human T lymphoblasts) for which only the distribution of FMNL1 is shown without quantification. No results presenting the effect of FMNL1 KO and expression of mutants in primary T cells are shown.

Referee is right regarding the extension of exosome secretion studies to primary human T lymphocytes. Unfortunately, it is well known that primary T lymphocytes are extremely difficult to transfect. Moreover, the expression of our large bi-cistronic large plasmids (>15 Kb) is very inefficient, coupled with the challenge of expressing large proteins, such as the 180 kDa YFP-FMNL1 chimeric variants. The convergence of all these undesirable factors synergistically hampers these studies and we have been unable to consistently achieve enough transfection efficiency to perform these experiments. However, the role of FMNL1 on MTOC/MVB polarization in Jurkat cells, confirmed in this manuscript, has been already extended to primary CD8+ T cell clones (DOI10.1016/j.immuni.2007.01.008). Given that exosome secretion requires

MTOC/MVB polarization both in Jurkat and primary T lymphoblasts (10.1038/cdd.2010.184, 10.3389/fimmu.2019.00851), this suggests FMNL1 may also control exosome secretion in primary T cells, although the formal demonstration will require further research.

A new sentence has been included in the Discussion to address this important point. Regarding the second request, we have quantified the images mentioned in Suppl. Fig. S7, and the percentages of fixed T cells showing FMNL1 accumulations at the immune synapse are included in the figure legend.

(2) Analysis in- depth of the defect in actin remodeling (quantification of the images, analysis of some key actors of actin remodeling) is still lacking. Only F-actin is shown, no attempt to look more precisely at actors of actin remodeling has been done.

The referee is right. Since we have obtained new results on the role of FMNL1 on actin remodeling, we have focused on this formin, which is already a key actor in this process. In this context, we have previously shown that the formin Dia1, another major actor of actin remodeling in T lymphocytes along with FMNL1 (DOI10.1016/j.immuni.2007.01.008), does not undergo phosphorylation upon PKC activation (Suppl. Fig. 5 in <https://doi.org/10.1080/20013078.2020.1759926>). Since our aim was to unravel the PKC-mediated pathway controlling actin remodeling, we have ruled out more studies on Dia1. Therefore, we have included a new sentence to emphasize the specific role of FMNL1 phosphorylation, but not Dia1, in this regard. Nonetheless, future studies aimed to identifying new important players in this or related pathways could offer significant insights.

(3) The defect in the secretion of extracellular vesicles is still very preliminary. Examples of STED images given by the authors are nice, yet no quantification is performed.

The referee is right regarding this point and we acknowledge this comment. Accordingly, we have now quantified the STED images and provided numerical data on the percentages of cells exhibiting the observed phenotypes (see the figure legend for Fig. 10).

(4) Results shown in Figure S12 on the colocalization of proteins phosphorylated on Ser/Thr are still not convincing. It seems indeed that "phospho-PKC" is labeling more preferentially the CMAC positive cells (Raji) than the Jurkat T cells. It is thus particularly difficult to conclude on the colocalization and even more on the recruitment of phosphorylated-FMNL1 at the IS. Thus, these experiments are not conclusive and cannot be the basis even for their cautious conclusion: "Although all these data did not allow us to infer that FMNL1b is phosphorylated at the IS due to the resolution limit of confocal and STED microscopes, the results are compatible with the idea that both endogenous FMNL1 and YFP-FMNL1bWT are specifically phosphorylated at the cIS".

The referee may be correct regarding the detail of the "phospho-PKC" labeling. However, it cannot be overlooked that Raji cells also contain proteins that are or may be potential PKC substrates. As a matter of fact, Raji cells also express FMNL1. In addition, MHCII triggering in B cells induces PKC activation (<https://doi.org/10.1002/eji.200323351>). Regarding which cell type is preferentially labeled, this is a variable topic depending on the analyzed synapse.

It is true that there are likely several PKC substrates, both in Jurkat in Raji cells, but our point is that one of these substrates either colocalizes with FMNL1 or is FMNL1 itself. We do not claim at any point that FMNL1 is the only PKC substrate, neither in Jurkat or in Raji cells.

Apparently, the referee has either overlooked our results or we did not emphasize them sufficiently. Our results effectively validated the PKC substrate antibody, both on endogenous phospho-FMNL1 and phospho-YFP-FMNL1 β by WB (Fig. 3). Moreover, the phospho-PKC does not recognize

YFP-FMNL1 β S1086A or S1086D variants (Fig. 3). Last, but not least, when FMNL1 is interfered in the Jurkat cell, the phospho-PKC does not colocalize with FMNL1, but it strongly

colocalizes at the synapse with expressed YFP-FMNL1 β WT in the Jurkat cell (Fig. S11). Indeed YFP-FMNL1 β belonged to the Jurkat cell. Taken together these results demonstrate: 1. the specificity of phospho-PKC antibody, 2. the phospho-PKC antibody certainly recognizes phosphorylated YFP-FMNL1 β but not its non-phosphorylatable mutant variants, 3. the colocalization of phospho-PKC with anti-FMNL1 is specific. We have included some sentences to clarify these points and to avoid possible misunderstandings by potential readers. We acknowledge the referee for his/her clarifying point, and we firmly believe our mentioned cautious conclusion is strictly correct, although we have tuned it to consider the possibility that a different PKC substrate could be closely associated to FMNL1, producing the observed colocalization: “Although all these data do not yet allow us to infer that FMNL1b is phosphorylated at the IS due to the resolution limits of super resolution microscopy and the possibility that another PKC substrate may be associated to FMNL1 or very close to FMNL1, in a strictly S1086-dependent manner”.

To clear any doubt regarding which cell is labelled with phospho-PKC, we have changed the lower panels in Suppl. Fig. S12, and now is more evident that FMNL1 and phospho-PKC belong to the Jurkat cell.

The study would benefit from a more careful statistical analysis. The dot plots showing polarity are presented for one experiment. Yet, the distribution of the polarity is broad. Results of the 3 independent experiments should be shown and a statistical analysis performed on the independent experiments.

The referee is right and we have now included further post-hoc analyses data (Tukey) at Suppl. Fig S13. Tukey’s test values were included for all the dot plot figures. We have not included all the plots from 3 different experiments since the manuscript already contains 10+12 multi panel figures and is too large. However, we have stated in the figure legend that these independent experiments are representative of the data obtained from 3 independent experiments. Referee’s consideration regarding the broad distribution of polarity data is correct. We included in the first version of the manuscript a sentence in this regard, that it may have been overlooked: “Remarkably, one important feature of the IS consists of both the onset of the initial cell-cell contacts and the establishment of a mature, fully productive IS, are intrinsically stochastic, rapid and asynchronous processes (87, 88) (43). Thus, the score of the PI corresponding to the distance of MTOC/MVB with respect the IS (42) may be contaminated by background MTOC/MVB polarization, in great part due to the stochastic nature of IS formation (87)”.

<https://doi.org/10.7554/eLife.96942.3.sa0>